Etl4^{lacZ}. As the expression patterns of *Etl4*^{lacZ} are quite similar to those in *Skt*^{Gt} mice and as *Etl4*^{lacZ} mice have similar kinks in the tail region (ZACHGO *et al.* 1998), the *lacZ* gene in the enhancer trap vector may be expressed under the control of this possible node/notochord enhancer. ZACHGO *et al.* (1998) reported that the *Etl4*^{lacZ} locus is localized ~0.75 cM distal to *Sd* and that the *Sd* phenotype is attenuated when *Etl4*^{lacZ} is present in *cis*. These results suggest that the possible enhancer sequence in the fourth intron of the *Skt* gene functions also as the enhancer for the *Sd* gene and that the insertion of an enhancer trap vector in the third intron, as found in the *Etl4*^{lacZ} line, may eliminate the enhancer function for the *Sd* gene, resulting in the attenuation of the *Sd* phenotype.

Future study on the functions of the Skt and Sd proteins may provide important clues for understanding the mechanisms for the development of notochordal cells and their differentiation into the nucleus pulposus cells.

We thank T. Iwamura, K. Miike, K. Haruna, and H. Hino for helpful and critical discussions and comments on the manuscript, and Michiyo Nakata and Ikuyo Kawasaki for technical assistance. This work was supported in part by a Grant-in-Aid on Priority Areas from the Ministry of Education, Science, Culture, and Sports of Japan and a grant from the Osaka Foundation for Promotion of Clinical Immunology.

LITERATURE CITED

ALFRED, J. B., K. RANCE, B. A. TAYLOR, S. J. PHILLIPS, C. M. ABBOTT *et al.*, 1997 Mapping in the region of Danforth's short tail and the localization of tail length modifiers. Genome Res. **7:** 108–117.

ALLEN, N. D., D. G. CRAN, S. C. BARTON, S. HETTEL, W. REIK *et al.*, 1988 Transgenes as probes for active chromosomal domains in mouse development. Nature **333:** 852–855.

ANG, S., and J. ROSSANT, 1994 HNF-3β is essential for node and notochord formation in mouse development. Cell **78:** 561–574.

ARAKI, K., T. IMAIZUMI, T. SEKIMOTO, K. YOSHINOBU, J. YOSHIMUTA *et al.*, 1999 Exchangeable gene trap using the Cre/mutated lox system. Cell. Mol. Biol. **45:** 737–750.

ASZODI, A., D. CHAN, E. HUNZIKER, J. F. BATEMAN and R. FASSLER, 1998 Collagen II is essential for the removal of the notochord and the formation of intervertebral discs. J. Cell Biol. **143:** 1399–1412.

BEHRENS, A., J. HAIGH, F. MECHTA-GRIGORIOU, A. NAGY, M. YANIV *et al.*, 2003 Impaired intervertebral disc formation in the absence of *Jun*. Development **130:** 103–109.

CHIANG, C., Y. LITINGTUNG, E. LEE, K. E. YOUNG, J. CORDEN *et al.*, 1996 Cyclopia and defective axial patterning in mice lacking Sonic hedgehog gene function. Nature **383:** 407–413.

CRICK, F. H., 1952 Is alpha-keratin a coiled coil? Nature **170:** 882–883.

DUNN, L. C., S. GLUECKSOHN-SCHOENHEIMER and V. BRYSON, 1940 A new mutation in the mouse affecting spinal column and urogenital system. J. Hered. **31:** 343–348.

GERARD, R. D., and Y. GLUZMAN, 1985 New host cell system for regulated simian virus 40 DNA replication. Mol. Cell. Biol. **5:** 3231–3240.

GOSSLER, A., A. L. JOYNER, J. ROSSANT and W. C. SKARNES, 1989 Mouse embryonic stem cells and reporter constructs to detect developmentally regulated genes. Science **244:** 463–465.

GRUNEBERG, H., 1953 Genetical studies on the skeleton of the mouse. VI. Danforth's short-tail. J. Genet. **51:** 317–326.

GRUNEBERG, H., 1958 Genetical studies on the skeleton of the mouse. XXII. The development of Danforth's short-tail. J. Embryol. Exp. Morphol. **6:** 124–148.

HOGAN, B., R. BEDDINGTON, F. COSTANTINI and E. LACY, 1994 *Manipulating the Mouse Embryo: A Laboratory Manual*, pp. 379–381. Cold Spring Harbor Laboratory Press, Cold Spring Harbor, NY.

KORN, R., M. SCHOOR, H. NEUHAUS, U. HENSELING, R. SONININEN *et al.*, 1992 Enhancer trap integrations in mouse embryonic stem cells give rise to staining patterns in chimaeric embryos with a high frequency and detect endogenous genes. Mech. Dev. **39:** 95–109.

KOZAK, M., 1996 Interpreting cDNA sequences: some insights from studies on translation. Mamm. Genome **7:** 563–574.

KUSANO, K. N. KAGAWA, M. SAKAGUCHI, T. OMURA and M. R. WATERMAN, 2001a Importance of a proline-rich sequence in the amino-terminal region for correct folding of mitochondrial and soluble microbial p450s. J. Biochem. **129:** 271–277.

KUSANO, K., M. SAKAGUCHI, N. KAGAWA, M. R. WATERMAN and T. OMURA, 2001b Microsomal p450s use specific proline-rich sequences for efficient folding, but not for maintenance of the folded structure. J. Biochem. **129:** 259–269.

LANE, P. W., and C. S. BIRKENMEISER, 1993 Urogenital syndrome (*us*): a developmental mutation on chromosome 2 of the mouse. Mamm. Genome **4:** 481–484.

LANGMAN, J., 1969 *Medical Embryology*, pp. 134–135. Williams & Wilkins, Baltimore.

LUPAS, A., 1996 Coiled coils: new structures and new functions. Trends Biochem. Sci. **21:** 375–382.

LUPAS, A., M. VAN DYKE and J. STOCK, 1991 Predicting coiled coils from protein sequences. Science **252:** 1162–1164.

MAATMAN, R., J. ZACHGO and A. GOSSLER, 1997 The Danforth's short tail mutation acts cell autonomously in notochord cells and ventral hindgut endoderm. Development **124:** 4019–4028.

NISHIZAKI, Y., K. SHIMAZU, H. KONDOH and H. SASAKI, 2001 Identification of sequence motifs on the node/notochord enhancer of Foxa2 (Hnf3β) gene that are conserved across vertebrate species. Mech. Dev. **102:** 57–66.

NIWA, H., K. YAMAMURA and J. MIYAZAKI, 1991 Efficient selection for high-expression transfectants with a novel eukaryotic vector. Gene **108:** 193–200.

PAAVOLA, L. G., D. B. WILSON and E. M. CENTER, 1980 Histochemistry of the developing notochord, perichordal sheath and vertebrae in Danforth's short-tail (*Sd*) and normal C57BL/6 mice. J. Emboryol. Exp. Morphol. **55:** 227–245.

PAULING, L., and R. B. COREY, 1953 Compound helical configurations of polypeptide chains: structure of proteins of the alpha-keratin type. Nature **171:** 59–61.

RUFAI, A., M. BENJAMIN and J. R. RALPHS, 1995 The development of fibrocartilage in the rat intervertebral disc. Anat. Embryol. **192:** 53–62.

SMITS, P., and V. LEFEBVRE, 2003 Sox5 and Sox6 are required for notochord extracellular matrix sheath formation, notochord cell survival and development of the nucleus pulposus of intervertebral discs. Development **130:** 1135–1148.

THEILER, K., 1988 Vertebral malformations. Adv. Anat. Embryol. Cell Biol. **112:** 1–99.

WILSON, V., L. MANSON, W. C. SKARNES and R. S. BEDDINGTON, 1995 The T gene is necessary for normal mesodermal morphogenetic cell movements during gastrulation. Development **121:** 877–886.

ZACHGO, J., R. KORN and A. GOSSLER, 1998 Genetic interactions suggested that Danforth's short tail (Sd) is a gain-of-function mutation. Dev. Genet. **23:** 86–96.

Communicating editor: C. A. KOZAK

Available online at www.sciencedirect.com
SCIENCE DIRECT
ELSEVIER
Biochemical and Biophysical Research Communications 341 (2006) 132–138
BBRC
www.elsevier.com/locate/ybbrc

Impaired expression of importin/karyopherin β1 leads to post-implantation lethality

Katsutaka Miura [a,1], Kumiko Yoshinobu [b], Takashi Imaizumi [a,1], Kyoko Haruna [a,c], Yoichi Miyamoto [d], Yoshihiro Yoneda [d], Naomi Nakagata [b], Masatake Araki [b], Taihei Miyakawa [e], Ken-ichi Yamamura [a], Kimi Araki [a,*]

[a] *Institute of Molecular Embryology and Genetics, Kumamoto University, Honjo 2-2-1, Kumamoto 860-0811, Japan*
[b] *Institute of Resource Development and Analysis, Kumamoto University, Honjo 2-2-1, Kumamoto 860-0811, Japan*
[c] *TransGenic Inc., 12-32 Hanabata-cho, Kumamoto 860-0806, Japan*
[d] *Department of Frontier Biosciences, Graduate School of Frontier Biosciences, Osaka University, Suita, Osaka 565-0871, Japan*
[e] *Department of Neuropsychiatry, Kumamoto University School of Medicine, Honjo 1-1-1, Kumamoto 860-8556, Japan*

Received 30 November 2005
Available online 6 January 2006

Abstract

Importin β1 (Impβ)/karyopherin β1 (Kpnb1) mediates the nuclear import of a large variety of substrates. This study aimed to investigate the requirement for the *Kpnb1* gene in mouse development, using a gene trap line, B6-CB-*Ayu8108*^{GtgeoIMEG} (*Ayu8108*^{geo}), in which the trap vector was inserted into the promoter region of the *Kpnb1* gene, but in reverse orientation of the *Kpnb1* gene. *Ayu8108*$^{geo/geo}$ homozygous embryos could develop to the blastocyst stage, but died before embryonic day 5.5, and expression of the *Kpnb1* gene in homozygous blastocysts was undetectable. We also replaced the *βgeo* gene with Impβ cDNA through Cre-mediated recombination to rescue Impβ expression. Homozygous mice for the rescued allele *Ayu8108*$^{Impβ/Impβ}$ were born and developed normally. These results demonstrated that the cause of post-implantation lethality of *Ayu8108*$^{geo/geo}$ homozygous embryos was impaired expression of the *Kpnb1* gene, indicating indispensable roles of Impβ1 in early development of mice.
© 2006 Elsevier Inc. All rights reserved.

Keywords: Importin β1; Gene trap; Cre/lox site-specific recombination; Embryonic lethal

Active nuclear import of proteins is a highly selective process involving specific recognitions between nuclear localization signals (NLS) and suitable receptors [1]. Importin/karyopherin β1 (Impβ) is a key player in nuclear protein import and mediates targeting of a canonical NLS substrate bound to an adaptor protein, importinα [2,3]. On the nuclear membrane, Impβ interacts with nuclear envelope-localized nuclear pore complexes (NPCs) and carries the importinα/cargo complex from the cytoplasm into the cell nucleus. In the nucleus, RanGTP, which exists predominantly in the nucleus, binds to Impβ and induces the release of import cargoes. Thereafter, individual importins are recycled back to the cytoplasm. Thus, Impβ is a critical component in mechanisms involved in targeting of the NLS substrate into the nucleus [4–6].

In addition to nuclear transport, Impβ has also been shown to play a role in regulation of spindle formation and of aster promoting activity (APA) during mitosis [7–10]. Two microtubule organizing components, NuMA and TPX2, which are retained in the nucleus during interphase, bind to Impβ via importinα during mitosis and are kept away from chromatin. RanGTP releases NuMA and TPX2 from importin α/β heterodimer around chromosomes and promotes spindle formation.

* Corresponding author. Fax: +81 96 373 6599.
E-mail address: arakimi@gpo.kumamoto-u.ac.jp (K. Araki).
[1] Present address: Kumamoto University Hospital, 1-1-1 Honjo, Kumamoto 860-8556, Japan.

0006-291X/$ - see front matter © 2006 Elsevier Inc. All rights reserved.
doi:10.1016/j.bbrc.2005.12.151

Impβ is the prototype of the karyopherin family including more than 20 members in mammals [11]. Ten of these members have been identified to have a role in nuclear import. In general, such importinβ family proteins function without the need of an adaptor protein and can directly interact with their substrates. To the best of our knowledge, only Impβ requires an adaptor, importinα, to bind to its cognate cargoes.

Extensive studies using cultured cells have clarified molecular mechanisms of nuclear transport. However, roles and functional redundancy of Impβ family members in vivo have been poorly studied. In *Drosophila*, Impβ mutant strains (*Ketel* mutations) have been isolated and analyzed [12–14]. Homozygous larvae for the loss-of-function *Ketel* allele die during the second larval instar, but on the other hand, homozygous somatic clones induced by mitotic recombination are viable in the follicle epithelium in wings and tergites. Since the *Ketel* gene is not expressed in larval and adult cells that are mitotically inactive, another import pathway might substitute for the function of Impβ in *Drosophila*.

In order to identify the requirement for the *importin/karyopherinβ1* (Kpnb1) gene in mouse development, we analyzed a *Kpnb1* mutant mouse line established by gene trapping [15]. The trap vector was inserted in the promoter region of the *Kpnb1* gene in the reverse orientation of the transcription of the *Kpnb1* gene, and expression of the *Kpnb1* gene from the mutated allele was severely decreased. Homozygous embryos could develop to the blastocyst stage, but died before embryonic day (E) 5.5, indicating that Impβ1 played an indispensable role in early development of mice.

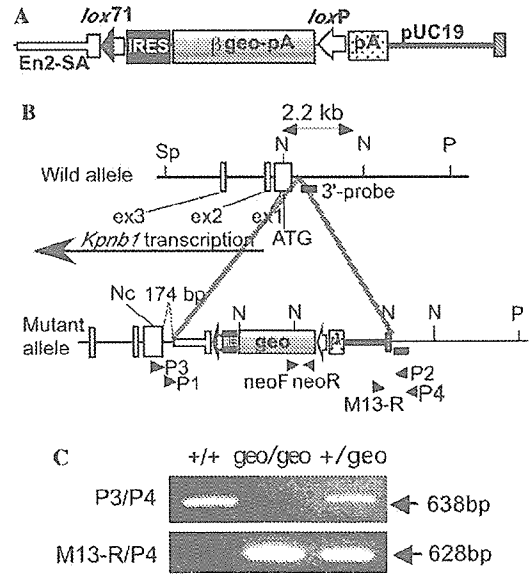

Fig. 1. Gene trap events in the Ayu8108 clone. (A) Structure of the trap vector, pU-hachi. The pU-hachi vector contains an IRES-βgeo-pA cassette flanked by *lox*71 and *lox*P to exchange the βgeo cassette into any DNA sequence through recombination by Cre. En2, the mouse *Engrailed 2* gene; SA, splice acceptor; pA, polyadenylation signal. (B) Integration pattern of the trap vector. Open boxes on the maps represent the first three exons of the *Kpnb1* gene. The trap vector was inserted 174 bp upstream from the first exon. The start codon and direction of transcription of the *Kpnb1* gene are indicated. The solid bar with "3'-probe" shows the probe used in Southern blotting for genotyping. Arrowheads indicate primers used for genotyping and RT-PCR. N, *Nco*I; Sp, *Sph*I; P, *Pst*I. (C) Genotyping by PCR. The primer pairs neo-F/neo-R and P1/P2 were used to detect the *Ayu8108*^{geo} and wild-type alleles, respectively.

Materials and methods

Isolation of ES clones and establishment of mutant mouse lines. The gene trap vector pU-hachi and isolation of trap clones were described previously [15]. The vector contained a splice acceptor region (SA) from the mouse *En-2* gene, *lox*71, the internal ribosomal entry site (IRES) from the encephalomyocarditis virus (ECMV), the *β-galactosidase/neomysin phosphotransferase fusion* gene (*βgeo*), *lox*P, the SV40 polyadenylation sequence (pA), and pUC19 (Fig. 1A). In order to replace the *βgeo* gene with the Impβ cDNA sequence, a replacement vector carrying *lox*66-Impβ cDNA–phosphoglycerate kinase 1 (PGK)–*puromycin resistant* (*Pac*) gene–*lox*P–pSP73 was constructed. Site-specific integration in trap clones mediated by Cre-recombinase was performed as described previously [15]. Chimeric mice were produced by aggregation of ES cells with eight-cell embryos of ICR mice (Nippon Clea, Tokyo, Japan), as described previously [16]. Chimeric male mice and their heterozygous progeny were backcrossed for five to eight generations to a C57BL/6J background.

Molecular cloning of flanking genomic region by plasmid rescue. Plasmid rescue was performed as described previously [15]. Genomic DNA of Ayu8108 ES cells was digested with *Pst*I or *Sph*I, followed by self-ligation, and introduction into *Escherichia coli* cells by electroporation. The recovered plasmids were mapped by restriction enzymes and sequenced using the dideoxy chain termination method using a BigDye Terminator Cycle Sequencing (Perkin-Elmer, Foster City, CA).

Genotyping of mice. Genomic DNA was isolated by proteinase K digestion, phenol–chloroform extraction, and ethanol precipitation from tail biopsies of newborn, E10.5 embryos, and E7.5 embryos.

For newborn mice and E10.5 embryos, Southern blot analysis was carried out. Seven micrograms of genomic DNA was digested with an appropriate enzyme, electrophoresed on 1% agarose gel, and blotted onto a nylon membrane (Roche Molecular Biochemicals, Mannheim, Germany). Probe preparation and hybridization were performed with the DIG DNA Labeling and Detection Kit (Roche).

For E7.5 embryos, PCR analysis was carried out. To identify the mutant allele, the primers neo-F (5'-AGAGGCTATTCGGCTATGAC-3') and neo-R (5'-CACCATGATATTCGGCAAGC-3') were used. PCR conditions were 30 cycles of 94 °C for 30 s, 58 °C for 30 s, and 72 °C for 60 s, using 0.5 U AmpliTaq DNA polymerase (Roche). To identify the wild allele, the primers P1 (5'-ATTGGCCGGACGGCTAGCGT-3') and P2 (5'-GCTGAGCCCGAAGGCCTTTA-3') were used. PCR conditions were 30 cycles of 94 °C for 30 s, 58 °C for 60 s, and 72 °C for 60 s, using 0.5 U LA *Taq* DNA polymerase (TaKaRa, Shiga, Japan).

For blastocysts and cultured embryos, individual embryos were lysed for 5 min in 2 μl of 0.005% SDS, 0.035 N NaOH, at 100 °C. After neutralization by adding 36 μl water, PCR was carried out using 5 μl of the extract. Primer pairs M13-R (5'-AGGAAACAGCTATGACCATGA-3') and P3(5'-GGTCACCACAAGCCCATTCA-3'), P3 and P4 (5'-GAACTCCTCGCTTCAGTTCT-3') were used to identify mutant and wild alleles, respectively. PCR conditions were 40 cycles of 94 °C for 30 s, 62 °C for 30 s, and 72 °C for 30 s, using 0.5 U LA *Taq* polymerase (TaKaRa).

Quantitative analysis of expression of the Kpnb1 gene. Ten micrograms total RNA was reverse-transcribed using Superscript II (Invitrogen, Carlsbad, CA) according to the manufacturer's instructions. Real-time quantitative reverse-transcription polymerase chain reaction (RT-PCR) was performed with a LightCycler instrument, using Faststart DNA

Master SYBR Green I Kit (Roche). PCRs were performed using B1 (5′-TAACCATCCTCGAGAAGACC-3′) and B2 (5′-ATCCCCTGGATT ATGGCAGT-3′) primers, and 40cycles of 95 °C for 30 s, 60 °C for 30 s, and 72 °C for 30 s.

Isolation and in vitro culture of blastocysts. Heterozygous female mice were superovulated and mated with heterozygous male mice, and 2-cell stage embryos were isolated and cultured in KSOM [17] medium for 2 days to the blastocyst stage. Individual blastocysts were transferred to single wells coated with gelatin in 15% FCS–DMEM. Plates were incubated and kept in a humid chamber at 37 °C, 5% CO_2 for 3 days.

Histological analysis of E5.5 embryos. Heterozygous and wild-type females were superovulated and mated with heterozygous males. Fertilized eggs were collected from the oviducts and transferred to foster mothers on the same day. Decidual swellings containing E5.5 embryos were dissected, fixed in 4% paraformaldehyde solution, and sectioned. Serial sections were stained with hematoxylin and eosin (H/E), and observed under a microscope.

RT-PCR analyses. Total RNA was isolated from individual blastocysts using the RNeasy Mini Kit (Qiagen, Valencia, CA) and suspended in 30 μl water. First-strand cDNA was synthesized using 9 μl RNA solution with oligo(dT) primers in a ThermoScript RT-PCR System (Invitrogen, Carlsbad, CA). One-twentieth volume of the first-strand reaction was used for PCR amplification. Expressions of the *βgeo* and *Kpnb1* genes were detected using primers neo-F and neo-R, and primers B3 (5′-CTCTTCA GAATGTTCTCCGG-3′) and B4 (5′-GATCTCCGCCCTTCAGTTAA-3′), respectively. Pericentriolar material-1 (PCM1) was used as internal positive control. Primers for PCM1 were 5′-GCGTTACCCAACTT AATC-3′ and 5′-TGTGAGCGAGTAACAACC-3′. Both PCR conditions were 40 cycles of 94 °C for 30 s, 58 °C for 30 s, and 72 °C for 30 s using 0.5 U LA *Taq* DNA polymerase (TaKaRa). In the case of adult mice, 10 μg of total RNA was used for first-strand cDNA synthesis using the SuperScript First-Strand Synthesis System for RT-PCR (Invitrogen). To detect expressions of the inserted Impβ cDNA and the endogenous *Kpnb1* gene, primers E3 (5′-GTTCGAGCTTGGAATTCATG-3′) and B5 (5′-CCGT CGAGCATTAGCATCAA-3′), and B3 and B6 (5′-CCTCTC ATTCCCAAGCATTC-3′) were used, respectively. PCR conditions were 35 cycles of 94 °C for 30 s, 58 °C for 60 s, and 72 °C for 60 s using 0.5 U AmpliTaq polymerase (Perkin-Elmer).

5-rapid amplification of cDNA ends (RACE) and 3′RACE analyses. Total RNA was prepared using Sepazol reagent (Nacalai Tesque, Kyoto, Japan), and mRNA was purified using the Oligotex-dT30 Super mRNA Purification Kit (TaKaRa). Reverse-transcription was performed with Thermoscript (Invitrogen) using primer E1 (5′-AGCAGTGAA GGCTGTGC-3′) for 5′RACE. The 5′RACE System for Rapid Amplification of cDNA Ends Reagent Assembly Ver. 2.0 (Invitrogen) was used according to the manufacturer's instructions, using the primer E2 (5′-CTT TGTTAGGGTTCTTCTTC-3′). Products were electrophoresed and subjected to Southern blotting using digoxigenin-ddUTP-labeled oligonucleotide probes for the SA sequence in the trap vector, prepared using the DIG Oligonucleotide 3′-End Labeling Kit (Roche). Hybridization with the probes was carried out overnight at 60 °C.

The downstream cDNA fragment containing a poly(A) stretch was obtained using 3′RACE System for Rapid Amplification of cDNA Ends (Invitrogen). First-strand cDNA was synthesized with a 3′RACE Adapter Primer using the Thermoscript RT-RCR System (Invitrogen) and two nested primers P5 (5′-CATTGGCCTGCGGCTTCA-3′) and P6 (5′-CGG CTTCAAGGTCCGGTT-3′). RACE products were cloned into pGEM-T vectors (Promega, Madison, WI) and sequenced.

Results

Analysis of the insertion event in Ayu8108 trap clone

Ayu8108 ES clone cells were isolated using gene trap screening with the pU-Hachi trap vector (Fig. 1A), which was designed for the exchangeable gene trap [15]. Southern blot analysis with a probe for the pUC vector fragment revealed a single copy integration of the vector (data not shown). Genomic DNA fragments flanking both the 5′ and 3′ ends of the integrated vector were obtained by the plasmid rescue method after removal of the *βgeo* sequence by Cre-mediated recombination [18]. Sequence analysis of the flanking genomic DNA and homology search in the GenBank database revealed that the trap vector was integrated into the promoter region of the *Kpnb1* gene. Although the transcription initiation site of the *Kpnb1* gene was not yet determined, several expression sequence tag (EST) sequences covering the 5′-region of the *Kpnb1* gene show 5′-ends at 290–323 bp upstream of the start codon of the *Kpnb1* gene. Therefore, in our study, the 5′-end of the BY740663 EST sequence, which has the most extended 5′-end, was considered as the *Kpnb1* transcription initiation site. The trap vector was integrated at 225 bp upstream of the first exon, however, direction of transcription of the *βgeo* was opposite to that of the *Kpnb1* gene (Fig. 1B). Deletion of genomic DNA at the integration site was only of 46 bp, and no deletion was found in the integrated trap vector.

Chimeric mice were produced by aggregation of Ayu8108 ES cells with morulae, and the trap mouse line designated as B6-CB-*Ayu8108*^{GtgeoIMEG} (*Ayu8108*^{geo}) was established.

Identification of the trapped transcript in the Ayu8108 line

The fact that the direction of transcription of the *βgeo* was opposite to that of the *Kpnb1* gene (Fig. 1) indicated the existence of another gene in the promoter region of the *Kpnb1* gene. In fact, ubiquitous expression of the trapped gene was observed by X-gal staining in E9.5 and E12.5 embryos (data not shown). Moreover, in adult mice, transcripts of the *βgeo* were detected in the brain, heart, lung, kidney, and testis using RT-PCR (data not shown).

To identify endogenous transcripts fused to the βgeo gene, we performed 5′RACE and obtained a clear single band (Fig. 2A). Sequence analysis revealed that transcription of the fusion transcripts started at 50 bp upstream from the insertion site, which corresponded to 124 bp upstream of the first exon of the *Kpnb1* gene, and spliced at a cryptic splice-donor site (position 52 in the pU-hachi sequence, GenBank Accession No. AB242616) within the intron of the trap vector to fuse the authentic splice acceptor (Fig. 2B). Then, 3′RACE was performed to obtain the whole transcript of the trapped gene, and a 1.3-kb product was obtained (GenBank Accession No. AB242615). As shown in Fig. 2C, the sequence was identical to the 3′-flanking genomic sequence of the trap vector. Homology search using BLAST programs [19] identified several mouse ESTs with high homology (>95%). However, in the 1.3-kb transcript, multiple stop codons appeared in all three frames, and no apparent ORF was found. Northern blot analysis was performed using both total and poly(A) RNAs from adult tissues and an RNA probe for

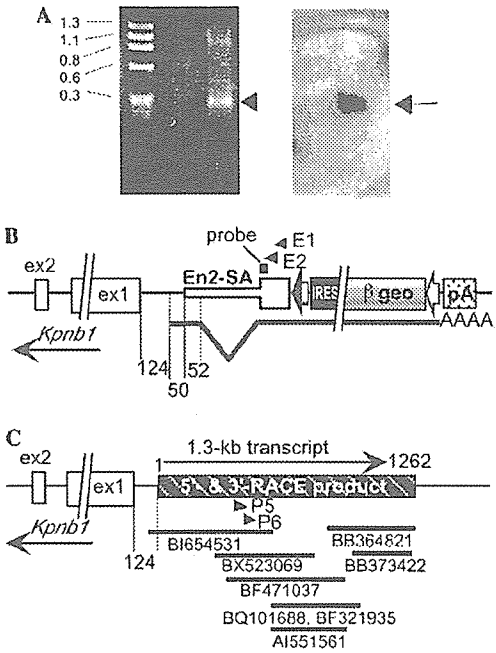

Fig. 2. Identification of the transcript trapped in the Ayu8108 clone. (A) 5′-RACE analysis of the Ayu8108 ES line. A single band (arrowhead) was obtained with E1 and E2 primers (left), and the product hybridized with an oligoprobe from the SA sequence (right, arrow), showing successful amplification of the fusion transcript with the SA sequence of the trap vector. (B) Schematic structure of transcription of the fusion transcript from the *Ayu8108*^{geo} mutant allele. Transcription started 124 bp upstream from the first exon of the *Kpnb1* gene and was spliced at a cryptic splice donor site in the intron sequence of the trap vector. (C) Transcription of the trapped gene in the wild allele. The 1.3-kb transcript identified by 5′- and 3′RACE is indicated by a thick box. The arrow on the box indicates the direction of transcription. Primers used for 3′-RACE are indicated by arrowheads. EST sequences from GenBank are shown under the map with their respective accession numbers.

the 1.3-kb product. However, only a faint signal was detected with total RNA, and no signal was obtained with poly(A) RNA (data not shown). Thus, in the Ayu8108 clones, we could not detect endogenous transcripts from the trapped gene. However, it was possible that a non-coding RNA gene was trapped.

Expression of the Kpnb1 gene is impaired in Ayu8108$^{+/geo}$ *mice*

Since the integration site of the trap vector was quite close to the first exon of the *Kpnb1* gene, it was expected that insertion would result in impaired expression of the *Kpnb1* gene, although direction of transcription was opposite. In order to examine expression levels of the *Kpnb1*gene in *Ayu8108*$^{+/geo}$ heterozygous mice, we performed real-time RT-PCR quantification in liver, kidneys, and testes of adult mice. As shown in Fig. 3, expression levels of the *Kpnb1* mRNA in *Ayu8108*$^{+/geo}$ mice were significantly lower (about 60–80%) than those of wild-type, indicating that integration of the trap vector produced a hypomorphic allele of the *Kpnb1*gene.

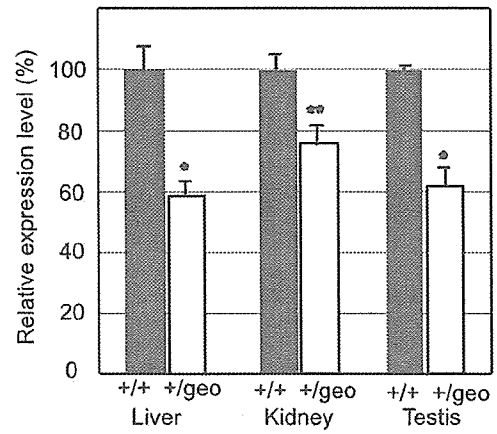

Fig. 3. Comparison of expression levels of the *Kpnb1* gene between wild-type and *Ayu8108*$^{+/geo}$ heterozygous mice by Real-time RT-PCR. Total RNAs from liver ($n = 6$), kidneys ($n = 6$), and testes ($n = 5$) of wild-type (+/+, black bars) and *Ayu8108*$^{+/geo}$ (+/geo, open bars) adult mice were used. In each tissue, relative expression level against average amount in wild-type mice is indicated with standard deviation. $^{*}p < 0.01$; $^{**}p < 0.05$ (Student's *t*-test).

Ayu8108$^{geo/geo}$ *homozygous embryos were lethal after implantation*

Ayu8108$^{+/geo}$ heterozygous mice were healthy in appearance and fertile. To investigate the phenotype of *Ayu8108*$^{geo/geo}$ homozygous mice, heterozygous mice were crossed, and neonates, E10.5 and E7.5 embryos, were genotyped by Southern blotting or PCR analysis (Fig. 1C). As shown in Table 1, no homozygous progeny was identified. Out of 62 deciduas obtained from E7.5, 27.4% of deciduas were empty, likely to correspond to missing homozygotes (Table 1), indicating that decreased expression of the *Kpnb1* gene caused embryonic lethality. To score rates of abortion in the uteri, heterozygous and negative littermate females were superovaluated and mated with heterozygous males. Fertilized eggs were then collected, and transferred into foster mothers on the same day, and then E5.5 deciduas were histologically analyzed. As shown in Table 2, in experiments with wild-type and heterozygous females, frequency of resorptions was 8.3% and 36.2%, respectively.

Table 1
Genotyping distribution of embryos and pups derived from heterozygous intercrosses

Age stage	+/+ (%)	+/geo, geo/+ (%)	geo/geo (%)	Resorbed (%)	Total
Blastocyst	6 (33.3)	9 (50.0)	3 (16.7)	—	18
Outgrowth	5 (20.0)	10 (40.0)	5 (20.0)	—	20
E7.5	18 (29.1)	27 (43.5)	0	17 (27.4)	62
E10.5	15 (37.5)	25 (62.5)	0	ND	40
Newborn	12 (33.3)	24 (66.7)	0	—	36

Embryos and newborn mice were genotyped by Southern blot analysis (newborn and 10.5 dpc), or by PCR analysis using P1/P2 and neo-F/R primers (7.5 dpc) or with M13-R, P3, and P4 primers (blastocysts and outgrowth blastocysts). ND, Not determined: although empty deciduas existed, their numbers were not counted.

Table 2
Frequency of resorptions of E5.5 embryos

Cross	Total No. of deciduas	No. of resorptions	Resorption frequency (%)
+/+ X +/geo	48	4	8.3
+/geo X +/geo	47	17	36.2

Fertilized eggs from the indicated crosses were transferred into oviducts. Then, at E5.5, deciduas were dissected, sectioned, and stained with hematoxylin and eosin to examine morphology of embryos. All viable embryos showed normal morphology.

The difference of 27.9% was expected to correspond to the rate of homozygotes, and no embryonal tissue was observed in the empty deciduas (data not shown). These results strongly suggested that all *Ayu8108*$^{geo/geo}$ homozygous embryos were lethal before E5.5.

To investigate whether homozygous embryos could survive to the blastocyst stage, two-cell stage embryos from heterozygous crosses were collected and cultured up to the blastocyst stage. All embryos showed normal morphology without any developmental delay. Each embryo was lysed and subjected to PCR for genotyping. At this stage, homozygous embryos were identified (Table 1). Then, growth potential of homozygous embryos was examined by in vitro culture on gelatin-coated culture slides for 3 days. All blastocysts obtained from heterozygous crosses hatched out of the zona pellucida and attached to the slides. Genotyping of explants identified 5 (20%) homozygotes (Table 1). These results suggested that *Ayu8108*$^{geo/geo}$ homozygous embryos could develop to the blastocyst stage (E3.5), and hatch out, but they died shortly after implantation by E5.5.

In order to examine expression of the *Kpnb1*gene at the blastocyst stage, RT-PCR analysis using individual blastocysts obtained from heterozygous crosses was performed. Fig. 4 depicts results of a typical experiment. In total, 70 blastocysts were examined, and 21 blastocysts (30%) showed wild-type expression pattern [βgeo(−)/Kpnb1(+)], 34 (49%) showed heterozygous expression pattern [βgeo(+)/Kpnb1(+)], and 15 (21%) showed homozygous expression pattern [βgeo(+)/Kpnb1(−)]. Results of genotyping and RT-PCR indicated that expression of the *Kpnb1* gene was undetectable by RT-PCR in *Ayu8108*$^{geo/geo}$ homozygous embryos.

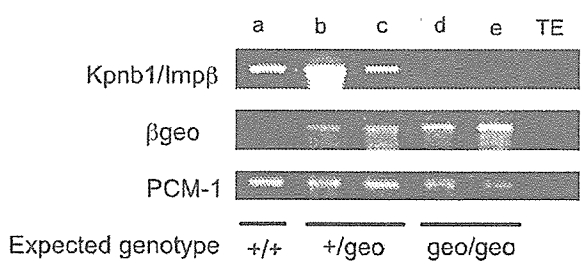

Fig. 4. RT-PCR analysis of individual blastocysts. Total RNAs from individual blastocysts (a–e) were subjected to RT-PCR to detect expression of the endogenous *Kpnb1* gene (upper panel) and the *βgeo* gene (middle panel). Detection of PCM-1 mRNA was performed as positive control (lower panel).

Expression of the Kpnb1 gene rescued post-implantation lethality

In *Ayu8108*$^{geo/geo}$ homozygous mice, expressions of the *Kpnb1* gene and of the 1.3-kb transcript were severely impaired by insertion of the trap vector. In order to determine what was responsible for lethality, we replaced the *βgeo* gene of the trap vector with Impβ cDNA, using the Cre/mutated *lox* recombination system as outlined in Fig. 5A. The inserted Impβ cDNA should be expressed under the control of the promoter for the 1.3-kb transcript, and production of the 1.3-kb transcripts should remain interrupted. After introduction of the replacement vector and of the Cre-expression vector [20] into Ayu8108 ES clones, 24 colonies were picked up, and 22 of 24 (90%) clones were shown to have the replaced alleles, *Ayu8108*$^{+/Impβ}$, by Southern blotting and PCR analyses (Fig. 5B). Then, the *Ayu8108*$^{+/Impβ}$ mouse line was established from one of the replaced clones through production of germline chimeras. Heterozygous *Ayu8108*$^{+/Impβ}$ mice were crossed, to obtain and examine phenotype of *Ayu8108*$^{Impβ/Impβ}$ homozygous mice. Genotype analysis (Figs. 1B and 5B) of 63 4-week-old offsprings identified 13 (21%) wild-type mice, 35 (56%) heterozygous mice, and 11 (17%) homozygous mice for the replaced allele, and all *Ayu8108*$^{Impβ/Impβ}$ homozygous mice appeared healthy. Expression of the endogenous *Kpnb1* gene and of the inserted Impβ cDNA was analyzed by RT-PCR using specific primer pairs for each transcript. As shown in Fig. 5C, expression of the integrated Impβ cDNA was detected in heterozygous and homozygous mice. Unexpectedly, the endogenous *Kpnb1* gene was expressed in *Ayu8108*$^{Impβ/Impβ}$ homozygous mice. This demonstrated that recovered Impβ expression from the inserted cDNA and endogenous *Kpnb1* gene rescued early embryonic lethality, and lethality was caused by impaired expression of the *Kpnb1* gene, but not of the 1.3-kb transcript.

Discussion

A hypomorphic allele of the mouse *Kpnb1* gene was generated by gene trap mutagenesis using ES cells. In heterozygous adult mice, expression level of the *Kpnb1* gene was reduced to about 60–70%, and in homozygous blastocysts, transcripts were not detected by RT-PCR. Homozygous blastocysts were able to grow on gelatin-coated slides, but homozygous implanted embryos died before E5.5 in vivo. These results indicated that Impβ protein was indispensable for the development of early stage embryos, and that any other importinβ family members could not compensate for nuclear import activity.

The developmental function of Impβ has been analyzed only in mutant *Drosophila* strains. In *Drosophila*, homozygous mutants could develop to the second larval instar

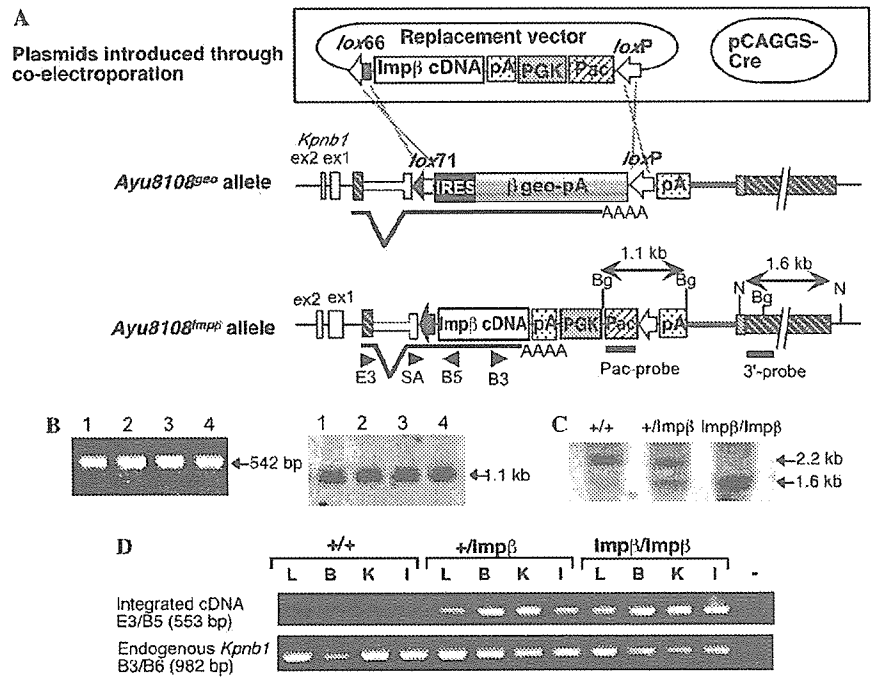

Fig. 5. Production and analysis of the *Ayu8108*^{Impβ} mouse line. (A) Site-specific replacement of the *βgeo* gene with a 2.6-kb Impβ cDNA sequence through Cre-mediated recombination. The replacement vector contains *lox*66-Impβ cDNA-pA-PGK promoter-*pac*-*lox*66 (top). Ayu8108 ES cells were co-electroporated together with the replacement vector and the Cre-expressing vector, pCAGGS-Cre. Through recombination between *lox* sites, the *βgeo* gene was replaced with the Impβ cDNA sequence (bottom). Striped boxes indicate transcribed genomic DNA regions for the 1.3-kb transcript. Replaced clones were selected in the presence of Puromycin (2 μg/ml). The integrated cDNA sequence was expressed as endogenous promoter activity which had driven the *βgeo* gene before replacement. Splicing patterns of transcripts for *βgeo* and integrated cDNA are shown under the maps. Primers used for confirmation of recombination and RT-PCR are indicated by arrowheads. Bg, *Bgl*II; N, *Nco*I. (B) Confirmation of targeted recombination at the *lox* sites. Results of representative 4 clones (1–4) are shown. Left, PCR with SA and B5 primers to detect the 5′-side junction. Right, Southern blot analysis with the Pac-probe and *Bgl*II digestion to detect the 3′-side junction. Bands with expected sizes were detected in both analyses. (C) Genotyping of the *Ayu8108*^{Impβ} mouse line. Tail DNA was digested with *Nco*I and hybridized with a 3′-probe. From the wild and *Ayu8108*^{Impβ} allele, a 2.2-kb band (Fig. 1B) and a 1.6-kb band were detected, respectively. (D) RT-PCR analysis of expression of the inserted or endogenous Impβ transcripts in each genotype. RT-PCR was performed using total RNAs from adult brain (B), kidneys (K), intestines (I), and lungs (L). To detect transcripts from the integrated Impβ cDNA and the endogenous *Kpnb1* gene, E3/B5 primer pair, and B3/B6 primer pair were used, respectively. B6 primer was in the 3′-untranslated region, therefore the B3/B6 primer pair can specifically detect endogenous *Kpnb1* expression. In homozygous *Ayu8108*$^{Impβ/Impβ}$ mice, both inserted Impβ cDNA and endogenous *Kpnb1* gene were expressed. −, template without RT reaction.

probably because of maternal accumulation of Impβ protein. In the case of importinβ-deficient eggs derived from germline chimeras carrying Impβ-deficient female germ cells, embryogenesis did not start at all [13]. Post-implantation lethality in our homozygous mutants for the Ayu8108 allele suggested that maternal Impβ mRNA or protein was present in mouse embryos, and that these might become depleted at the time of implantation.

In the Ayu8108 trap line, the trap vector was inserted in the promoter region of the *Kpnb1* gene in the reverse orientation. Recent genome and expression studies have revealed that many pairs of genes were driven by the same promoter sequence but in reverse direction [21,22], and that there were also non-coding RNA genes of unknown functions [23,24]. We identified a 1.3-kb product as the transcript of the trapped gene in Ayu8108 clones, but no ORF was found, and its expression was under detectable levels using northern blotting. As *Ayu8108*$^{Impβ/Impβ}$ homozygous mice were viable and healthy by expressing Impβ, but not the 1.3-kb transcript, the 1.3-kb transcript might not have a significant function in development. Yet, the 1.3-kb transcript might be a non-coding RNA of unknown function.

pU-hachi was constructed as an exchangeable gene trap vector using the Cre/mutant lox system. In this study, we used this system to insert the Impβ cDNA sequence, and we successfully identified the responsible gene for the early embryonic lethal phenotype. We clearly showed that Impβ was essential for early development in mice. Since there are many overlapping genes, insertion of a targeting vector may often result in disruptions of two genes. Our exchangeable system is expected to be a useful tool for analysis of such overlapping genes.

At present, we do not know why endogenous expression of the *Kpnb1* gene in the *Ayu8108*^{Impβ} allele recovered. We presume that there may be inhibitory element(s) for transcription in the IRES-βgeo sequence. It is known that the IRES sequence is quite GC rich and forms a complex secondary structure [25]. We have also produced the IRES-βgeo deleted allele by mating a Cre-expressing transgenic mouse line [26]. Homozygous mice for the IRES-βgeo

deleted allele were also viable and expressed the endogenous *Kpnb1* gene (data not shown). This supported the hypothesis of the existence of inhibitory elements. However, Impβ expression level from the *Ayu8108*^{Impβ}allele seemed to be lower than that of the wild-type allele, because we could not obtain compound heterozygous mice carrying both the *Ayu8108*^{geo} and the *Ayu8108*^{Impβ} alleles. Since we produced several alleles showing different expression levels of the *Kpnb1* gene, further analyses using these alleles would reveal the minimum requirements of Impβ expression level for development.

Acknowledgments

We thank Ms Y. Mine, R. Minato, and I. Kawasaki for their technical assistance. This study was supported in part by a Grant-in-Aid on Priority Areas from the Ministry of Education, Science, Culture and Sports of Japan, and a grant from the Osaka Foundation of Promotion of Clinical Immunology.

References

[1] C. Dingwall, R.A. Laskey, Nuclear targeting sequences—a consensus? Trends Biochem. Sci. 16 (1991) 478–481.
[2] D. Gorlich, S. Prehn, R.A. Laskey, E. Hartmann, Isolation of a protein that is essential for the first step of nuclear protein import, Cell 79 (1994) 767–778.
[3] N. Imamoto, T. Tachibana, M. Matsubae, Y. Yoneda, A karyophilic protein forms a stable complex with cytoplasmic components prior to nuclear pore binding, J. Biol. Chem. 270 (1995) 8559–8565.
[4] A. Harel, D.J. Forbes, Importin beta: conducting a much larger cellular symphony, Mol. Cell 16 (2004) 319–330.
[5] E. Conti, E. Izaurralde, Nucleocytoplasmic transport enters the atomic age, Curr. Opin. Cell Biol. 13 (2001) 310–319.
[6] Y. Yoneda, Nucleocytoplasmic protein traffic and its significance to cell function, Genes Cells 5 (2000) 777–787.
[7] O.J. Gruss, R.E. Carazo-Salas, C.A. Schatz, G. Guarguaglini, J. Kast, M. Wilm, N. Le Bot, I. Vernos, E. Karsenti, I.W. Mattaj, Ran induces spindle assembly by reversing the inhibitory effect of importin alpha on TPX2 activity, Cell 104 (2001) 83–93.
[8] M.V. Nachury, T.J. Maresca, W.C. Salmon, C.M. Waterman-Storer, R. Heald, K. Weis, Importin beta is a mitotic target of the small GTPase Ran in spindle assembly, Cell 104 (2001) 95–106.
[9] C. Wiese, A. Wilde, M.S. Moore, S.A. Adam, A. Merdes, Y. Zheng, Role of importin-beta in coupling Ran to downstream targets in microtubule assembly, Science 291 (2001) 653–656.
[10] M. Ciciarello, R. Mangiacasale, C. Thibier, G. Guarguaglini, E. Marchetti, B. Di Fiore, P. Lavia, Importin beta is transported to spindle poles during mitosis and regulates Ran-dependent spindle assembly factors in mammalian cells, J. Cell Sci. 117 (2004) 6511–6522.
[11] A.C. Strom, K. Weis, Importin-beta-like nuclear transport receptors, Genome Biol. 2 (2001), REVIEWS3008.
[12] M. Lippai, L. Tirian, I. Boros, J. Mihaly, M. Erdelyi, I. Belecz, E. Mathe, J. Posfai, A. Nagy, A. Udvardy, E. Paraskeva, D. Gorlich, J. Szabad, The Ketel gene encodes a *Drosophila* homologue of importin-beta, Genetics 156 (2000) 1889–1900.
[13] L. Tirian, J. Puro, M. Erdelyi, I. Boros, B. Papp, M. Lippai, J. Szabad, The Ketel(D) dominant-negative mutations identify maternal function of the *Drosophila* importin-beta gene required for cleavage nuclei formation, Genetics 156 (2000) 1901–1912.
[14] G. Timinszky, L. Tirian, F.T. Nagy, G. Toth, A. Perczel, Z. Kiss-Laszlo, I. Boros, P.R. Clarke, J. Szabad, The importin-beta P446L dominant-negative mutant protein loses RanGTP binding ability and blocks the formation of intact nuclear envelope, J. Cell Sci. 115 (2002) 1675–1687.
[15] K. Araki, T. Imaizumi, T. Sekimoto, K. Yoshinobu, J. Yoshimuta, M. Akizuki, K. Miura, M. Araki, K. Yamamura, Exchangeable gene trap using the Cre/mutated lox system, Cell. Mol. Biol. (Noisy-le-grand) 45 (1999) 737–750.
[16] H. Shimada, T. Kaname, M. Suzuki, Y. Hitoshi, K. Araki, T. Imaizumi, K. Yamamura, Comparison of ES cell fate in sandwiched aggregates and co-cultured aggregates during blastocyst formation by monitored GFP expression, Mol. Reprod. Dev. 52 (1999) 376–382.
[17] G.T. Erbach, J.A. Lawitts, V.E. Papaioannou, J.D. Biggers, Differential growth of the mouse preimplantation embryo in chemically defined media, Biol. Reprod. 50 (1994) 1027–1033.
[18] K. Araki, M. Araki, K. Yamamura, Targeted integration of DNA using mutant lox sites in embryonic stem cells, Nucleic Acids Res. 25 (1997) 868–872.
[19] S.F. Altschul, W. Gish, W. Miller, E.W. Myers, D.J. Lipman, Basic local alignment search tool, J. Mol. Biol. 215 (1990) 403–410.
[20] K. Araki, M. Araki, J. Miyazaki, P. Vassalli, Site-specific recombination of a transgene in fertilized eggs by transient expression of Cre recombinase, Proc. Natl. Acad. Sci. USA 92 (1995) 160–164.
[21] N. Adachi, M.R. Lieber, Bidirectional gene organization: a common architectural feature of the human genome, Cell 109 (2002) 807–809.
[22] S. Katayama, Y. Tomaru, T. Kasukawa, K. Waki, M. Nakanishi, M. Nakamura, H. Nishida, C.C. Yap, M. Suzuki, J. Kawai, H. Suzuki, P. Carninci, Y. Hayashizaki, C. Wells, M. Frith, T. Ravasi, K.C. Pang, J. Hallinan, J. Mattick, D.A. Hume, L. Lipovich, S. Batalov, P.G. Engstrom, Y. Mizuno, M.A. Faghihi, A. Sandelin, A.M. Chalk, S. Mottagui-Tabar, Z. Liang, B. Lenhard, C. Wahlestedt, Antisense transcription in the mammalian transcriptome, Science 309 (2005) 1564–1566.
[23] S.R. Eddy, Non-coding RNA genes and the modern RNA world, Nat. Rev. Genet. 2 (2001) 919–929.
[24] P. Carninci, T. Kasukawa, S. Katayama, J. Gough, M.C. Frith, N. Maeda, R. Oyama, T. Ravasi, B. Lenhard, C. Wells, R. Kodzius, K. Shimokawa, V.B. Bajic, S.E. Brenner, S. Batalov, A.R. Forrest, M. Zavolan, M.J. Davis, L.G. Wilming, V. Aidinis, J.E. Allen, A. Ambesi-Impiombato, R. Apweiler, R.N. Aturaliya, T.L. Bailey, M. Bansal, L. Baxter, K.W. Beisel, T. Bersano, H. Bono, A.M. Chalk, K.P. Chiu, V. Choudhary, A. Christoffels, D.R. Clutterbuck, M.L. Crowe, E. Dalla, B.P. Dalrymple, B. de Bono, G. Della Gatta, D. di Bernardo, T. Down, P. Engstrom, M. Fagiolini, G. Faulkner, C.F. Fletcher, T. Fukushima, M. Furuno, S. Futaki, M. Gariboldi, P. Georgii-Hemming, T.R. Gingeras, T. Gojobori, R.E. Green, S. Gustincich, M. Harbers, Y. Hayashi, T.K. Hensch, N. Hirokawa, D. Hill, L. Huminiecki, M. Iacono, K. Ikeo, A. Iwama, T. Ishikawa, M. Jakt, A. Kanapin, M. Katoh, Y. Kawasawa, J. Kelso, H. Kitamura, H. Kitano, G. Kollias, S.P. Krishnan, A. Kruger, S.K. Kummerfeld, I.V. Kurochkin, L.F. Lareau, D. Lazarevic, L. Lipovich, J. Liu, S. Liuni, S. McWilliam, M. Madan Babu, M. Madera, L. Marchionni, H. Matsuda, S. Matsuzawa, H. Miki, F. Mignone, S. Miyake, K. Morris, S. Mottagui-Tabar, N. Mulder, N. Nakano, H. Nakauchi, P. Ng, R. Nilsson, S. Nishiguchi, S. Nishikawa, et al., The transcriptional landscape of the mammalian genome, Science 309 (2005) 1559–1563.
[25] S.K. Jang, E. Wimmer, Cap-independent translation of encephalomyocarditis virus RNA: structural elements of the internal ribosomal entry site and involvement of a cellular 57-kD RNA-binding protein, Genes Dev. 4 (1990) 1560–1572.
[26] K. Araki, M. Araki, K. Yamamura, Site-directed integration of the cre gene mediated by Cre recombinase using a combination of mutant lox sites, Nucleic Acids Res. 30 (2002) e103.

© 2006 Wiley-Liss, Inc.

genesis 44:57–65 (2006)

TECHNOLOGY REPORT

Optimized β-Galactosidase Staining Method for Simultaneous Detection of Endogenous Gene Expression in Early Mouse Embryos

Satoshi Kishigami,[1] Yoshihiro Komatsu,[1] Haruko Takeda,[1] Aya Nomura-Kitabayashi,[1] Yasutaka Yamauchi,[2] Kuniya Abe,[2] Ken-ichi Yamamura,[2] and Yuji Mishina[1]*

[1]Laboratory of Reproductive and Developmental Toxicology, National Institute of Environmental Health Sciences, Research Triangle Park, North Carolina

[2]Institute of Molecular Embryology and Genetics, Kumamoto University, Kumamoto, Japan

Received 30 November 2005; Accepted 7 December 2005

Summary: β-Galactosidase (β-gal) is one of the popular reporters for detecting the expression of endogenous or exogenous genes. Here we report 6-chloro-3-indoxyl-beta-D-galactopyranoside (S-gal) is more sensitive for β-gal activity than 5-bromo-4-chloro-3-indolyl-beta-D-galactoside (X-gal), particularly during the early developmental stages of mouse embryos. Further, we successfully combined β-gal staining with S-gal and in situ hybridization using DIG-labeled probes in both whole and sections of early stage embryos due to the sensitivity and color compatibility of S-gal. genesis 44:57–65, 2006. © 2006 Wiley-Liss, Inc.

Key words: beta-galactosidase; in situ hybridization; X-gal; S-gal

The *lacZ* that encodes β-galactosidase (β-gal) has been widely used as a reporter gene in the developmental biology field from *Drosophila* to mammals because of its high sensitivity and ease of detection. In the mouse, *lacZ* has been variously used for analysis of gene expression by knocking it into the targeted gene locus, detection of gene recombination by Cre-loxP, and detection of embryonic stem (ES) cell derivatives in chimeric analysis. In these contexts, double staining for β-gal activity and in situ hybridization can provide a powerful technique to examine the expression pattern of endogenous genes with monitoring of β-gal activity in the same specimen. This method was originally developed in *Drosophila* (Cubas *et al.*, 1991), then subsequently applied to other organisms such as the mouse (Tajbakhsh and Houzelstein, 1995). Recently, this technique has been combined with various other methods, such as double-stranded RNA interference (Mellitzer *et al.*, 2002). However, because a similar color is produced by β-gal activity using 5-bromo-4-chloro-3-indolyl-beta-D-galactoside (X-gal; dark blue) and in situ hybridization by DIG-labeled probes using nitro-blue tetrazolium (NBT)/5-bromo-4-chloro-3-indolyl phosphate (BCIP; purple), there are often difficulties in distinguishing these two stainings in the same tissue or cells; for example, this double-staining method is applicable to chimeras to evaluate the effect of the degree of chimerism by β-gal staining on other endogenous gene expressions (Ang *et al.*, 1994; Rhinn *et al.*, 1999).

To overcome such difficulties for double staining of β-gal activity and in situ hybridization, we tried using a different substrate, 6-chloro-3-indoxyl-beta-D-galactopyranoside (S-gal, MW 329.74) instead of X-gal (MW 408.63) in order to develop a compatible color with the purple staining for in situ hybridization by NBT/BCIP. S-gal shows a pink/magenta color after reaction, and has been used recently for the detection of β-gal activity (Baker *et al.*, 1999; Varlet *et al.*, 1997). However, these two substrates have never been compared for their sensitivity to detect β-gal activity. Therefore, we first compared the sensitivity of S-gal with X-gal, the most popular substrate for detection of β-gal activity. To this end, males heterozygous for ROSA26 (Zambrowicz *et al.*, 1997), which express β-gal ubiquitously, were bred with wildtype Swiss females, and embryos were obtained from embry-

The first two authors contributed equally to this work.

Current address for S. Kishigami: RIKEN Center for Developmental Biology, 2-2-3 Minatojima-minamimachi, Chuo-ku, Kobe, Hyogo 650-0047, Japan.

Current address for H. Takeda: Genetique Factorielle et Moleculaire, Faculte de Medecine Veterinaire, Universite de Liege B43, Bd de Colonster, 20, 4000 Liege, Belgium.

Current address for K. Abe: BioResource Center, RIKEN Tsukuba Institute, 3-1-1 Koyadai, Tsukuba, Ibaraki 305-0074, Japan.

*Correspondence to: Y. Mishina, LRDT, NIEHS, 111 Alexander Dr., RTP, NC 27709.

E-mail: mishina@niehs.nih.gov

Contract grant sponsor: Intramural Research Program of the NIH, National Institute of Environmental Health Sciences; Contract grant sponsor: Japan Society for the Promotion of Science (fellowship to S.K.).

Published online in Wiley InterScience (www.interscience.wiley.com).

DOI: 10.1002/gene.20186

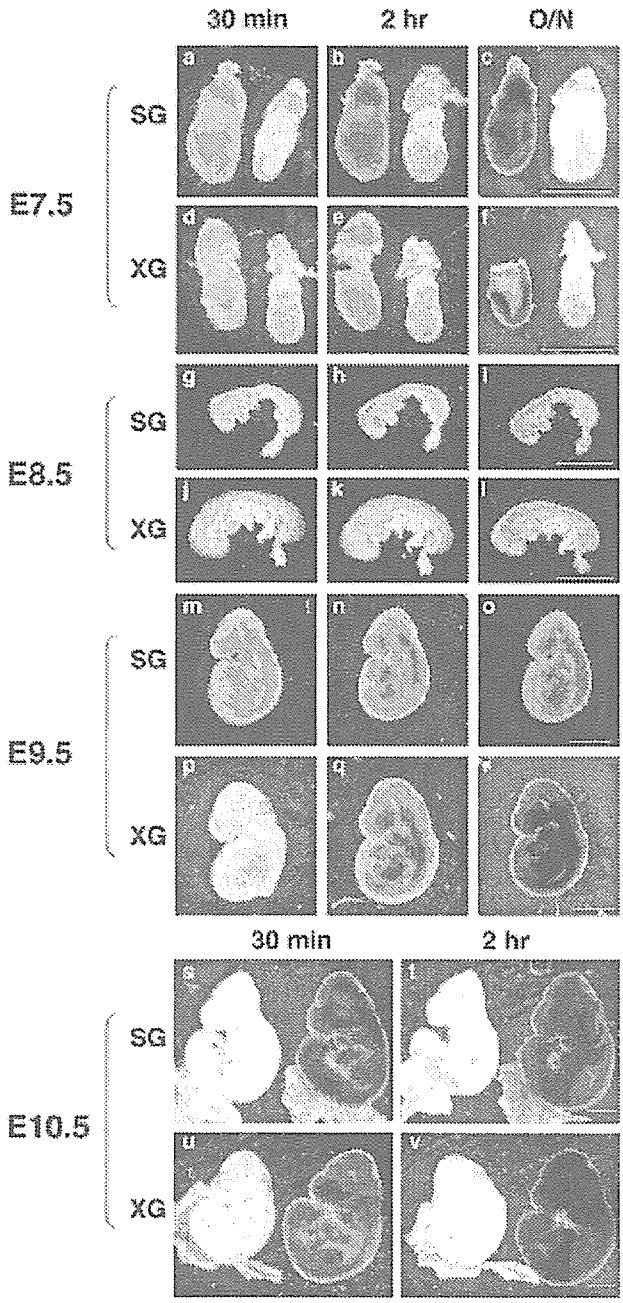

FIG. 1. Comparison of the sensitivity of S-gal and X-gal at E7.5–10.5. Embryos that carried *ROSA26* were fixed and stained with either 1 mg/ml of X-gal (XG) or S-gal (SG) at 37°C. Color development is depicted at 30 min, 2 h, and overnight after starting the reaction. Embryos on the right in panels **a–f** and those on the left in panels **s–v** are wildtype as controls. Early head fold stage embryos were used as E7.5. Scale bar = 1 mm.

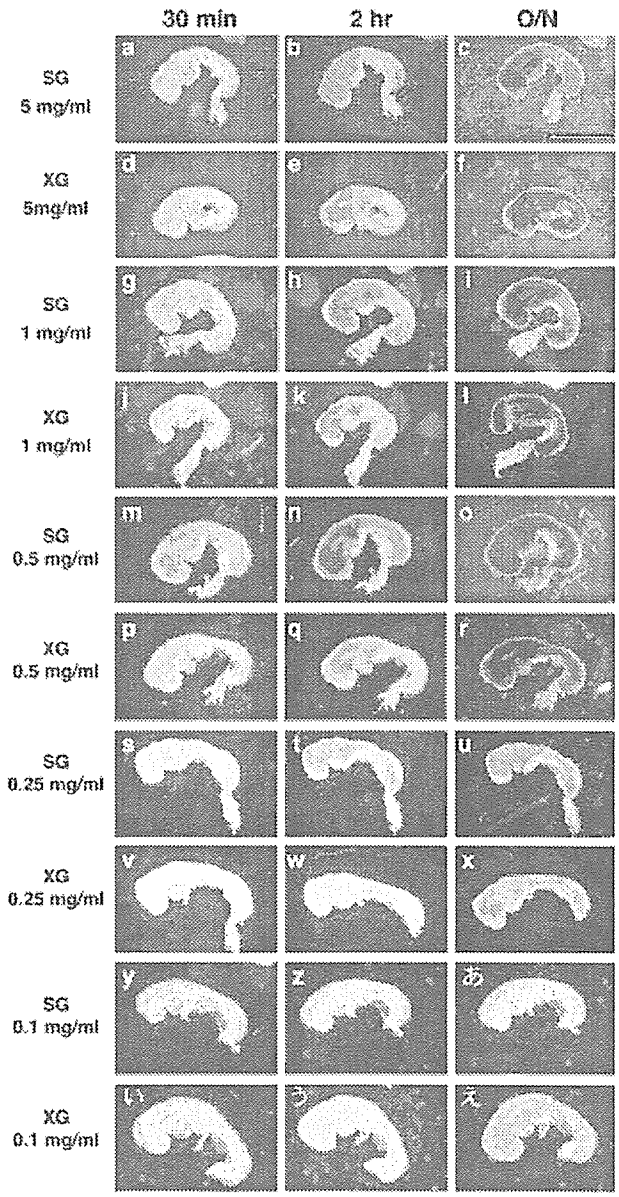

FIG. 2. Comparison of the sensitivity of S-gal and X-gal at different concentrations. E8.5 embryos of *ROSA26* at the 10-somite stage were stained with the indicated concentration of either X-gal (XG) or S-gal (SG) at 37°C. Color development is depicted at 30 min, 2 h, and overnight after starting the reaction. Scale bar = 1 mm.

onic day 7.5 (E7.5) to E10.5. Embryos were incubated either with 1 mg/ml of X-gal or S-gal at 37°C and color development was monitored. As shown in Figure 1 for E7.5–10.5, all stages of embryos stained with S-gal developed a magenta color within 30 min of incubation, whereas color development for embryos stained with X-gal took longer. This trend was more prominent in early stage embryos. Embryos stained with a lower concentration of S-gal also showed detectable color development in 30 min (Fig. 2m,s,y). Staining with 5 mg/ml of X-gal still took 2 h of incubation to develop a visible color level (Fig. 2d–f). Interestingly, no difference of incuba-

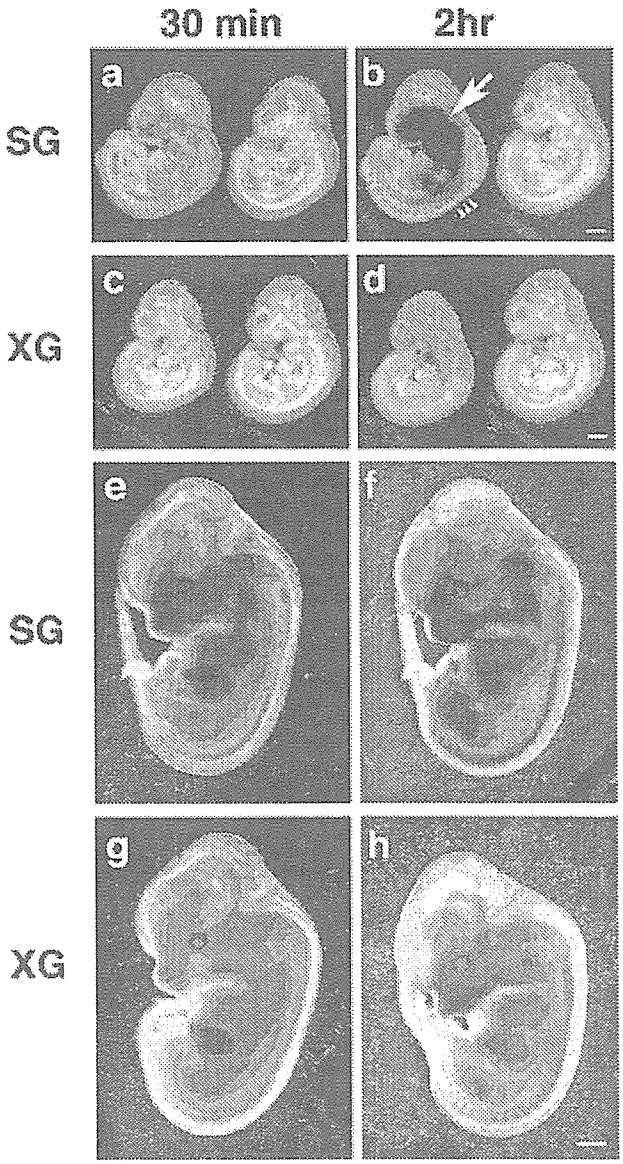

FIG. 3. Comparison of the sensitivity of S-gal and X-gal for detection of Cre recombinase activity. ROSA-reporter embryos that carry P0-Cre transgene were dissected at E10.5 (**a–d**) or E12.5 (**e–h**) and stained with either 1 mg/ml of S-gal (SG) or X-gal (XG). Embryos on the right in panels **a–d** are ROSA-reporter embryos without carrying P0-Cre transgene. Arrow, staining in a craniofacial region; arrowheads, staining in dorsal root ganglia. Scale bar = 1 mm. [Color figure can be viewed in the online issue, which is available at www.interscience.wiley.com.]

tion time to develop the color was observed for embryos later than E10.5 (Fig. 1s–v). This shortening of incubation time with S-gal will be of great advantage for double staining with in situ hybridization because degradation of RNA may be minimized. Furthermore, this result suggests that, if the incubation time to stain embryos with X-gal is short, analysis of gene expression by β-gal staining might miss the low expression of genes in early mouse embryos, which may lead to misinterpretation of gene functions.

This shorter incubation time with S-gal, particularly in early stage embryos, may suggest the ability of S-gal to detect β-gal activity at very low levels. This prompted us to examine whether β-gal activity induced by Cre recombinase could be detected by S-gal in a more sensitive manner than by X-gal soon after the expression of Cre recombinase. To confirm this, we used a *ROSA26* reporter strain, in which a *lacZ* expression cassette with a nuclear translocation signal (a nuclear-localized LacZ, nuclear LacZ hereafter) is used (Soriano, 1999), and a *P0-Cre* transgenic line that expressed Cre in a neural crest-specific manner (Yamauchi *et al.*, 1999). In this line, Cre recombinase expression starts as early as E9.5 in migrating neural crest cells. As shown in Figure 3, in E10.5 embryos a magenta color was detected in neural crest derivatives such as the craniofacial region and dorsal root ganglion as early as 30 min after incubation with S-gal (Fig. 3a,b). Overnight staining was required to obtain a similar pattern of staining using X-gal (Fig. 3c,d and not shown). In E12.5 embryos, there is less difference between S-gal and X-gal, and staining in the dorsal root ganglia was detected within 2 h using X-gal (Fig. 3e–h). Thus, even if these two substrates require different incubation times for the fully stained embryos, the fully stained embryos with either substrate reach the same pattern.

Since S-gal develops a magenta color, it can be combined with authentic in situ methods using DIG-labeled probes that typically develop a purple color with NBT/BCIP. Actually, we successfully detected the expression of *Msx1* with whole-mount in situ hybridization after staining with S-gal for 30 min (Fig. 4a). We also confirmed this with several other probes including *lefty1, lefty2, shh*, and *Pitx2* (data not shown). It was noted that there was no significant difference of time for developing a purple color for these hybridizations with and without the β-gal staining procedure, suggesting no significant degradation of endogenous mRNA during the short time incubation for β-gal staining.

We also recently demonstrated that this method was able to be applied successfully for evaluation of the relationship between the contribution of ES cells to chimeric embryos and alteration of the expression of endogenous genes (Kishigami *et al.*, 2004). *Acvr1* (alternatively known as *Alk2*) encodes a type I receptor for BMPs and homozygous mutant embryos die soon after gastrulation (Gu *et al.*, 1999; Mishina *et al.*, 1999). This early lethality was rescued by a chimeric situation that consisted of wildtype extraembryonic tissues and *Acvr1* mutant ES cells (Gu *et al.*, 1999; Mishina *et al.*, 1999). To evaluate the relationship between the contribution of ES cells and gene expression, we generated chimeric embryos by injecting *Acvr1* mutant ES cells carrying *ROSA26* into wildtype blastocysts. Levels of contribution of ES cells were evaluated by S-gal staining immediately after dissection (Fig. 4b) and whole-mount in situ hybrid-

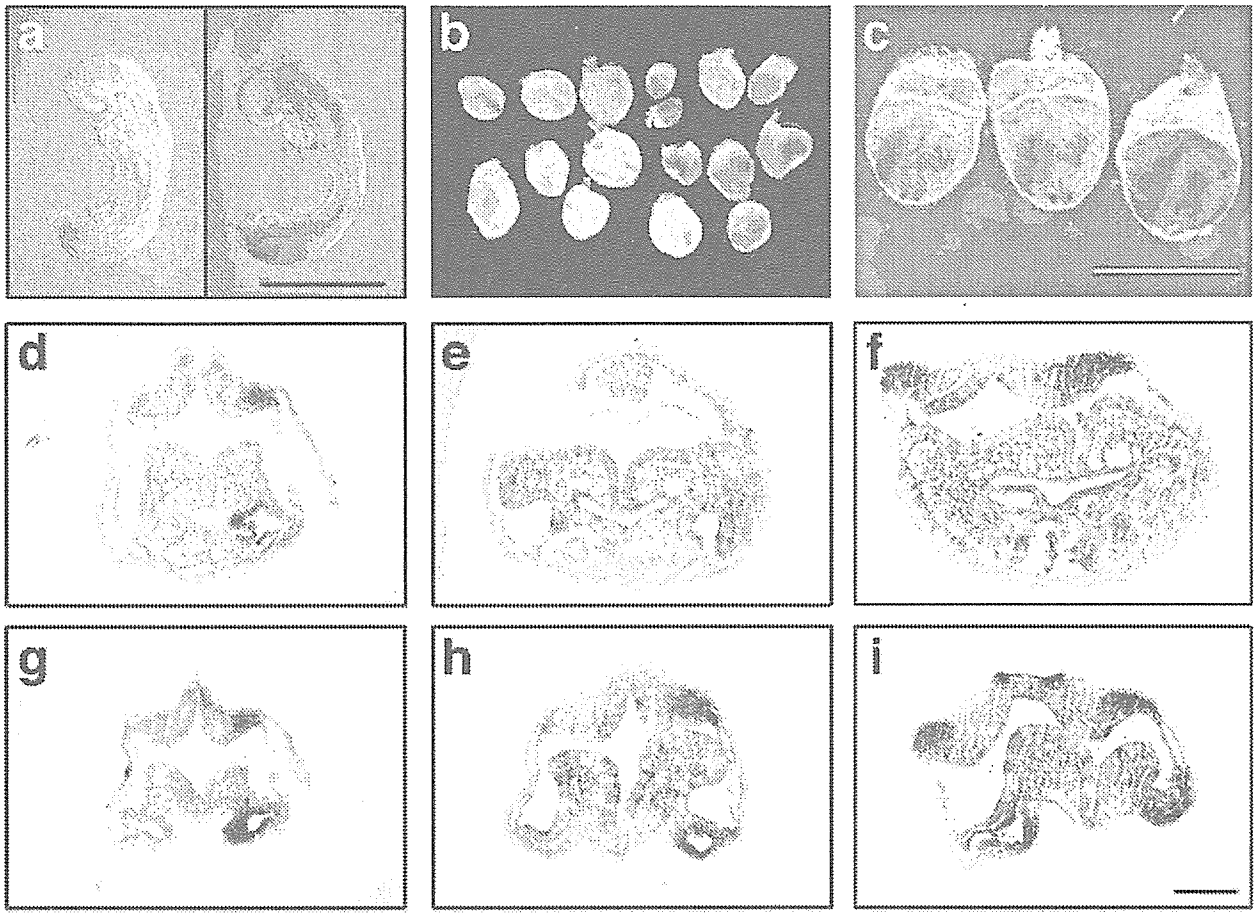

FIG. 4. Dual detection of β-gal activity and gene expression in whole embryos after staining with S-gal. Embryos stained with S-gal for 30 min at 37°C for magenta color development were subjected to whole-mount in situ hybridization with DIG-labeled RNA probes combined with NBT/BCIP for purple color development. **a:** Detection of *Msx1* expression in E8.5 embryos (7–8-somite stage) without (**a**, left) or with (**a**, right) *ROSA26*. **b:** A typical example of validation of chimeric production using S-gal, dissected at E7.5. **c:** Detection of *nodal* expression in different contribution levels of chimeras for *Acvr1* mutation (E7.5), posterior view (no, middle, and high contribution from left to right). **d–i:** 7-μm transverse sections of the embryos shown in **c**. Two sections in the embryonic regions close to the extraembryonic boundary (**d–f**) and close to the distal end (**g–i**) are shown. Note posterior bilateral expression of *nodal* in the lateral plate mesoderm of a high contribution chimera (**f,i**). Scale bars = 1 mm (**a,c**), 200 μm (**d–i**).

ization was performed. It is a practical advantage that the numbers of chimeric embryos and the degree of the contribution of ES cells can be known at the time of dissection, and desirable numbers of chimeric embryos can be pooled for in situ hybridization. Alterations of *nodal* expression patterns were observed in mutant chimeras depending on the level of contribution of the *Acvr1* mutant ES cells (Fig. 4c) (Kishigami *et al.*, 2004). Using sections, we demonstrated that observation at the tissue level of expression was possible (Fig. 4d–i).

Because β-gal used in the original ROSA26 strain stays in the cytoplasm, cellular levels of observation whether one particular cell is LacZ-positive or not become difficult if the expression level of an endogenous gene is high. To overcome this potential problem, first we examined if nuclear LacZ showed a confined staining pattern in the nucleus. We bred a ROSA reporter strain with P0-Cre mice, stained with S-gal, set up the whole-mount in situ hybridization, and subsequently made paraffin sections. However, because of the relatively harsh condition of the whole-mount in situ procedure, β-gal staining in the nuclei was not clearly detected (data not shown). Therefore, we modified the procedure to make paraffin sections immediately after staining with S-gal, and in situ hybridization was subsequently carried out on the sectioned materials. First, we compared the β-gal staining pattern of nuclear LacZ between X-gal and S-gal. On 7-μm sections, signals were able to be clearly detected as dot-like staining in the dorsal root ganglia (DRG), but not neural tube corresponding to the Cre expression pattern in P0-Cre mice after 2 h incubation with S-gal (Fig. 5e), which is consistent with the previous report

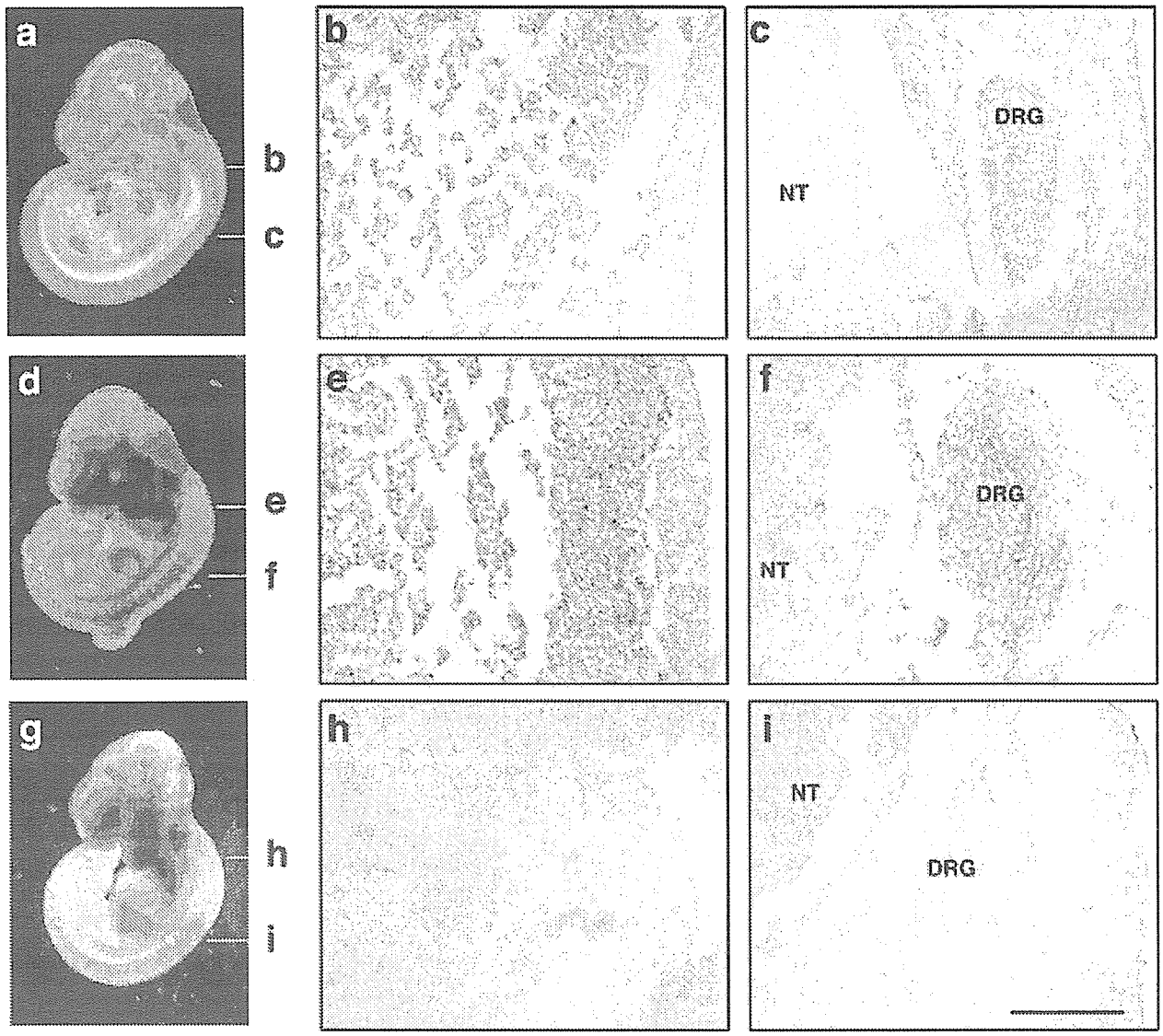

FIG. 5. Comparison of staining pattern of nuclear lacZ using S-gal and X-gal. ROSA-reporter mice were bred with P0-Cre transgenic mice and embryos were dissected at E10.5 and stained with 1 mg/ml of S-gal or X-gal, them paraffin sections were made. **a–c:** Stained with S-gal for 30 min. **d–f:** Stained with S-gal for 2 h. **g–i:** Stained with X-gal for 2 h. **b,e,h:** Sections at the level of branchyal arch. **c,f,i:** Sections contain dorsal root ganglia. NT, neural tube; DRG, dorsal root ganglion. Scale bar = 100 μm. [Color figure can be viewed in the online issue, which is available at www.interscience.wiley.com.]

(Ito *et al.*, 2003). On the other hand, 2 h incubation with X-gal did not produce the clear image of a dot-like structure (Fig. 5h). Note that even cytosolic LacZ produced a dot-like structure to some extent when S-gal was used as the substrate, depending on LacZ expression, which may represent that some amount of cytosolic LacZ is localized in the nuclei (data not shown). For dual detection of β-gal activity and endogenous gene expression, we bred ROSA-reporter mice with Mox2-Cre for ubiquitous expression of nuclear LacZ. Embryos were dissected at E10.5, stained with S-gal, sectioned, and followed by in situ hybridization using a probe for Fgf8. In this modified procedure, β-gal activity was also observed as several spots in each cell, conceivably corresponding to the nuclear structure found in hematoxylin-eosin staining (Fig. 6j,l). After in situ hybridization, β-gal signal still remained as spots that were distinguishable from cytoplasmic staining of *Fgf8* (Fig. 6m,n).

In order to confirm the advantage of S-gal at the later embryonic stages, we made cryosections and subsequently compared the time course of color development between S-gal and X-gal using E16.5 embryos. As shown

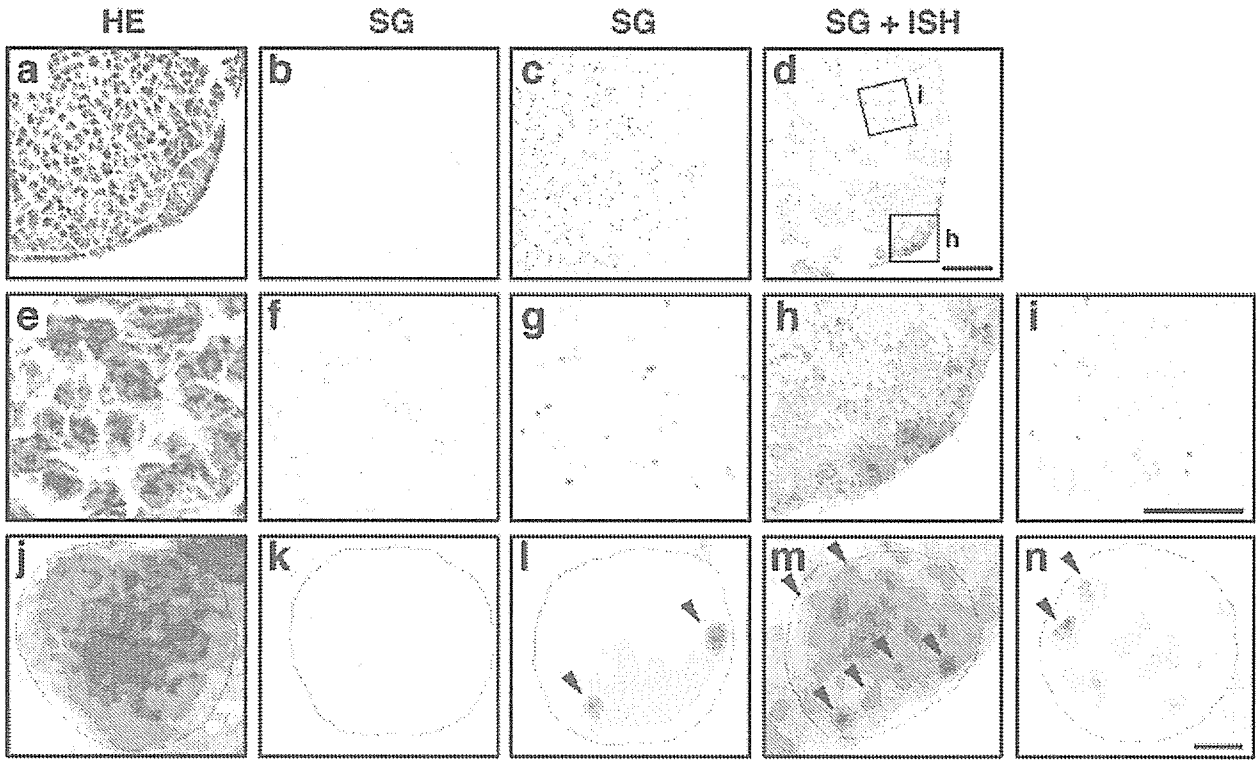

FIG. 6. Dual detection of β-gal activity and gene expression at the cellular level on paraffin sectioned materials. Embryos that express LacZ with a nuclear localization signal were dissected at E10.5, stained with 1 mg/ml of S-gal, and 6-μm paraffin sections of hindlimb were made. **a–d:** Low-magnification image of hindlimb. **e–i:** High-magnification image of **a–d. j–n:** Single cell view of **e–i.** Cell boundary is outlined by thin lines. **a,e,j:** Hematoxylin and eosin (HE) staining. Nuclei are stained as blue by hematoxylin. **b,c,f,g,k,l:** Sections from S-gal-stained embryos not carrying (**b,f,k**) or carrying (**c,g,l**) *Mox2-Cre* transgene. Note that the S-gal stain (magenta color) is confined in the cell nucleus. **d,h,i,m,n:** Adjacent sections of **c** were hybridized with a DIG-labeled RNA probe for *Fgf8*. In situ signal (blue color) was observed in the cell cytoplasmic region, whereas S-gal signal was localized in cell nucleus (arrowheads). High magnification of panel **d** where positive or negative *Fgf8* signals are shown in **h** and **m**, and **i** and **n**, respectively. Scale bars = 50 μm (**a–d**), 25 μm (**e–i**), 2 μm (**j–n**).

in Figure 7, sections stained with either X-gal or S-gal started to develop a color in 30 min; however, at 2 h S-gal stain produced a stronger signal than X-gal stain in pituitary (Fig. 7e–h), where P0-Cre was expressed (Yamauchi *et al.*, 1999). As seen in sectioned materials after whole-mount staining (Figs. 5, 6), we also observed that S-gal and X-gal stain had dot signals in a part of the cell nucleus, as previously reported (Ito *et al.*, 2003). Next, we investigated the detailed staining pattern of S-gal and in situ hybridization in cryosections. At E14.5, expression of the *Msx1* gene was restricted to the mesenchyme surrounding the incisor (Ferguson *et al.*, 2000; Tucker *et al.*, 1998). Also, typical in situ hybridization signals in cranial mesenchyme were found in the cell cytoplasmic region (Ding *et al.*, 2004). A magenta color, which derived from the S-gal stain, was observed in the cell nucleus (Fig. 8c, red arrowheads). On the other hand, a plexus pattern of purple in situ colors was seen in the cell cytoplasmic region (Fig. 8f, yellow arrows) and was able to be distinguished from the dotty staining of magenta color (Fig. 8f, red arrowheads). These results demonstrated that the detection of β-gal activity using S-gal and expression of an endogenous gene was able to be simultaneously monitored in the same cell if nuclear LacZ was used.

We successfully demonstrated that S-gal can be used for more applications than X-gal because of the color of the product and its higher sensitivity. In conclusion, we recommend that the choice between these two substrates, S-gal and X-gal, for detection of β-gal activity depend both on embryonic stages and color compatibility in mice.

MATERIALS AND METHODS

Breeding Mice

To obtain early stage embryos, male mice heterozygous for *ROSA26* (Zambrowicz *et al.*, 1997) were bred with wildtype females and vaginal plugs were subsequently checked. To detect Cre activity, male mice carrying a *P0-Cre* transgene (Yamauchi *et al.*, 1999) were bred with

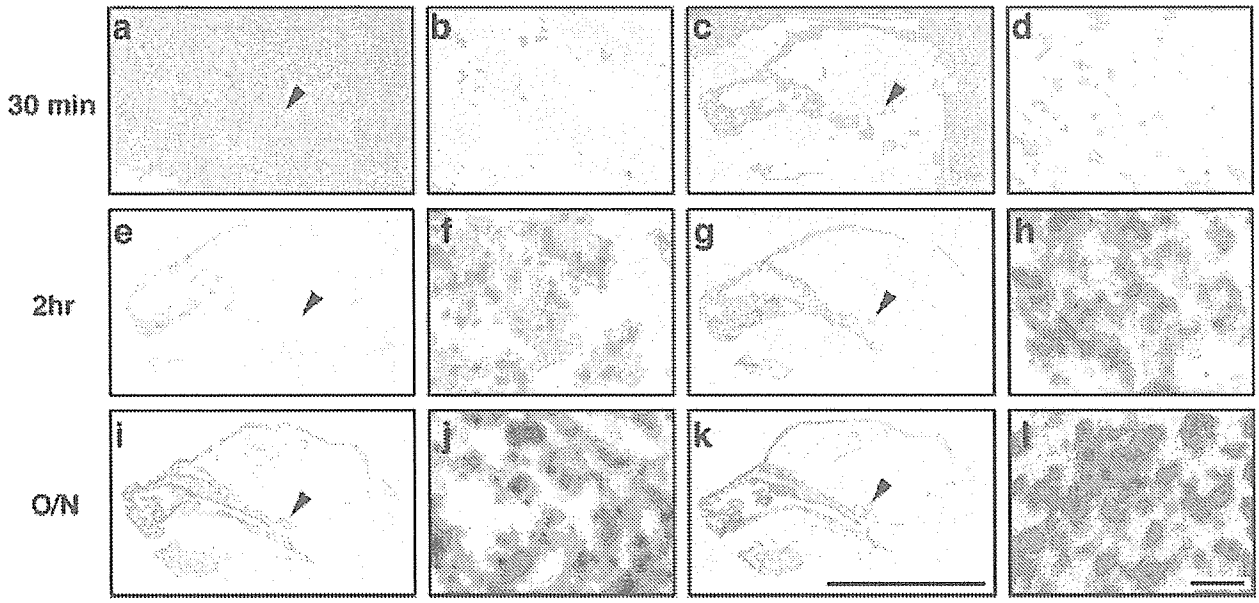

FIG. 7. Comparison of X-gal and S-gal stain on time course dependency. X-gal and S-gal staining pattern on each time course. 30 min (**a–d**), 2 h (**e–h**), and overnight (**i–l**) color development. Low magnification for a whole view of craniofacial sagittal section at E16.5 (**a,c,e,g,i,k**). High magnification for pituitary area where P0-Cre is expressed (**b,d,f,h,j,l**). Note that S-gal stain developed stronger signal than X-gal stain at 2 h (**e–h**). Scale bars = 5 mm (**a,c,e,g,i,k**), 50 μm (**b,d,f,h,j,l**).

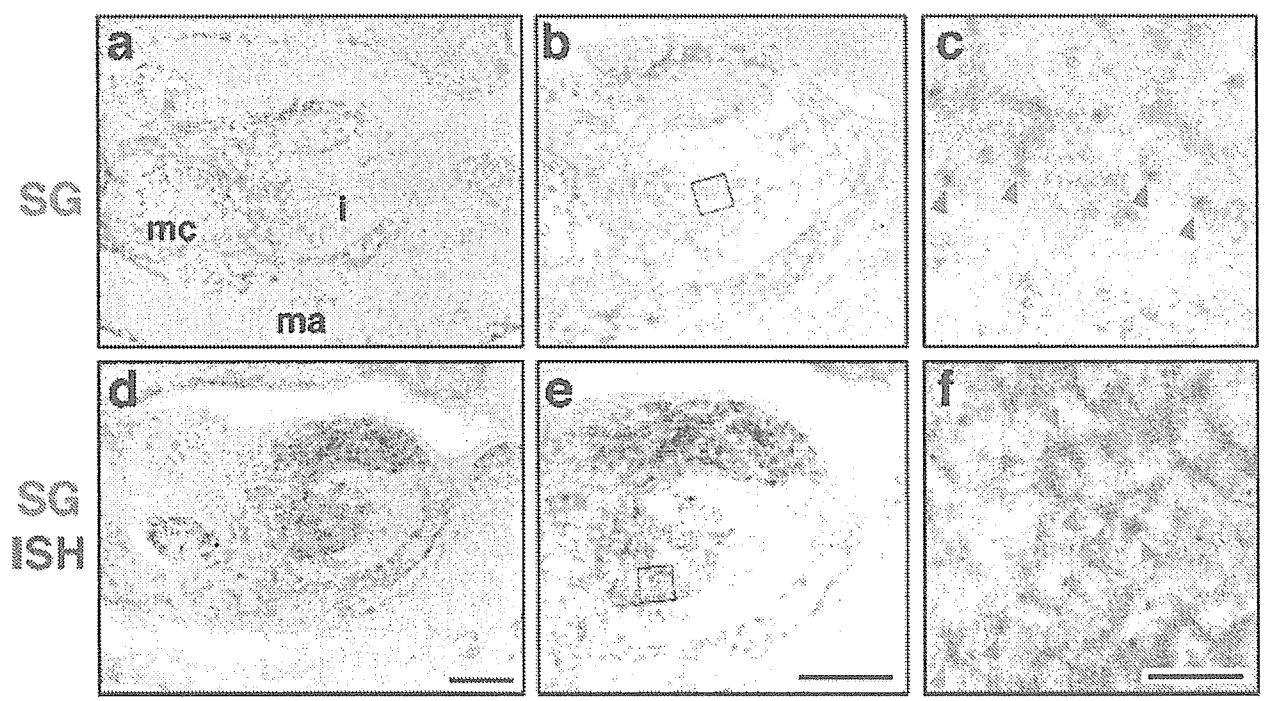

FIG. 8. Dual detection of β-gal activity and gene expression at the cellular level on cryosectioned materials. S-gal staining and in situ hybridization signal were monitored by magenta and purple color, respectively, in surrounded mesenchyme of incisor region at E14.5. **a–c:** Sections stained with 1 mg/ml of S-gal for 2 h. **d–f:** S-gal-stained sections followed by in situ hybridization using a DIG-labeled probe for *Msx1*. Note that S-gal stain was confined in nucleus as dotty signal (red arrowheads), whereas in situ signals were detected as a plexus pattern of purple colors on each cell (yellow arrows). ma, mandible; mc, Meckel's cartilage; i, incisor. Scale bars = 500 μm (**a,b,d,e**), 50 μm (**c,f**).

females that were homozygous for *ROSA26* reporter (Soriano, 1999). Establishment of mutant ES cell lines for *Alk2/Acvr1* and generation of chimeric embryos were described previously (Kishigami *et al.*, 2004; Mishina *et al.*, 1999). All mouse experiments were performed in accordance with institute guidelines covering the humane care and use of animals in research.

β-Gal Staining Followed by Whole-Mount In Situ Hybridization

After dissection, embryos were fixed with 4% paraformaldehyde for 5 min at 4°C, washed three times with phosphate-buffered saline (PBS), and stained with either 1 mg/ml of 6-chloro-3-indoxyl-beta-D-galactopyranoside (Salmon-beta-D-galactoside, MW 329.74; Biosynth, Staad, Switzerland; cat. #C5000) or 5-bromo-4-chloro-3-indolyl-beta-D-galactoside (X-gal, MW 408.63; Sigma, St. Louis, MO; cat. #B-4252), in 100 mM sodium phosphate buffer (pH 7.5), 0.1% sodium deoxycholate, 0.2% Nonidet P-40, 2 mM magnesium chloride, 5 mM potassium ferricyanide, and 5 mM potassium ferrocyanide at 37°C. For combination with whole-mount in situ hybridization, embryos stained with 1 mg/ml of S-gal for 30 min at 37°C were refixed with 4% paraformaldehyde overnight at 4°C and subjected to whole-mount in situ hybridization according to the protocol described previously (Conlon and Rossant, 1992). After color development, embryos were fixed in Bouin's fixative, dehydrated, and embedded in paraffin. Seven-μm-thick transverse sections were cut for histological observation.

β-Gal Staining Using Nuclear-LacZ Followed by In Situ Hybridization on Sectioned Materials

Mice homozygous for ROSA-Reporter (Soriano, 1999) were bred with Mox2-Cre transgenic mice that expressed Cre in the epiblast-specific manner (Tallquist and Soriano, 2000) or P0-Cre transgenic mice that expressed Cre in the neural crest-specific manner (Yamauchi *et al.*, 1999). By this means, embryos start to express β-galactosidase with a nuclear localization signal in the tissues where Cre is expressed. For both cases, embryos were dissected at E10.5, stained with 1 mg/ml of X-gal or S-gal, and subsequently 6-μm paraffin sections were made. In situ hybridization using digoxygenin-labeled RNA probe was carried out according to a nonradioactive protocol (Lindahl *et al.*, 1997). For cryosections, embryos were dissected at E14.5 or E16.5, 14-μm sections were made, and subsequently stained for β-gal activity according the method described by Chai *et al.* (2000) with modifications. In brief, dissected embryos were fixed with 4% paraformaldehyde overnight, subsequently soaked with 20% sucrose in PBS, and embedded in Optimal Cutting Temperature (O.C.T.) in liquid nitrogen. Fourteen-μm sections were cut, washed with PBS at room temperature, soaked with 100 mM sodium phosphate buffer (pH 7.5), 0.1% sodium deoxycholate, 0.2% Nonidet P-40, 2 mM magnesium chloride, 5 mM potassium ferricyanide, and 5 mM potassium ferrocyanide for 10 min at room temperature. Sections were subsequently stained with 1 mg/ml of X-gal or S-gal at 37°C. An S-gal-stained section was immediately used for in situ hybridization according to the nonradioactive protocol (Lindahl *et al.*, 1997).

ACKNOWLEDGMENTS

We thank Drs. Michael Kuehn, Michael Rauchman, and Thomas Gridley for in situ probes, and Drs. E. Mitch Eddy and Manas K. Ray for helpful comments on the article. We also thank Greg Scott and Toni Ward for assistance in the mouse activity and Kuniko Kishigami for encouragement.

LITERATURE CITED

Ang SL, Conlon RA, Jin O, Rossant J. 1994. Positive and negative signals from mesoderm regulate the expression of mouse Otx2 in ectoderm explants. Development 120:2979–2989.

Baker JC, Beddington RS, Harland RM. 1999. Wnt signaling in Xenopus embryos inhibits bmp4 expression and activates neural development. Genes Dev 13:3149–3159.

Chai Y, Jiang X, Ito Y, Bringas P Jr, Han J, Rowitch DH, Soriano P, McMahon AP, Sucov HM. 2000. Fate of the mammalian cranial neural crest during tooth and mandibular morphogenesis. Development 127:1671–1679.

Conlon RA, Rossant J. 1992. Exogenous retinoic acid rapidly induces anterior ectopic expression of murine Hox-2 genes in vivo. Development 116:357–368.

Cubas P, de Celis JF, Campuzano S, Modolell J. 1991. Proneural clusters of achaete-scute expression and the generation of sensory organs in the Drosophila imaginal wing disc. Genes Dev 5:996–1008.

Ding H, Wu X, Bostrom H, Kim I, Wong N, Tsoi B, O'Rourke M, Koh GY, Soriano P, Betsholtz C, Hart TC, Marazita ML, Field LL, Tam PP, Nagy A. 2004. A specific requirement for PDGF-C in palate formation and PDGFR-alpha signaling. Nat Genet 36:1111–1116.

Ferguson CA, Tucker AS, Sharpe PT. 2000. Temporospatial cell interactions regulating mandibular and maxillary arch patterning. Development 127:403–412.

Gu Z, Reynolds EM, Song J, Lei H, Feijen A, Yu L, He W, MacLaughlin DT, van den Eijnden-van Raaij J, Donahoe PK, Li E. 1999. The type I serine/threonine kinase receptor ActRIA (ALK2) is required for gastrulation of the mouse embryo. Development 126:2551–2561.

Ito Y, Yeo JY, Chytil A, Han J, Bringas P Jr, Nakajima A, Shuler CF, Moses HL, Chai Y. 2003. Conditional inactivation of Tgfbr2 in cranial neural crest causes cleft palate and calvaria defects. Development 130:5269–5280.

Kishigami S, Yoshikawa S, Castranio T, Okazaki K, Furuta Y, Mishina Y. 2004. BMP signaling through ACVR1 is required for left-right patterning in the early mouse embryo. Dev Biol 276:185–193.

Lindahl P, Karlsson L, Hellstrom M, Gebre-Medhin S, Willetts K, Heath JK, Betsholtz C. 1997. Alveogenesis failure in PDGF-A-deficient mice is coupled to lack of distal spreading of alveolar smooth muscle cell progenitors during lung development. Development 124:3943–3953.

Mellitzer G, Hallonet M, Chen L, Ang SL. 2002. Spatial and temporal 'knock down' of gene expression by electroporation of double-stranded RNA and morpholinos into early postimplantation mouse embryos. Mech Dev 118:57–63.

Mishina Y, Crombie R, Bradley A, Behringer RR. 1999. Multiple roles for activin-like kinase-2 signaling during mouse embryogenesis. Dev Biol 213:314–326.

Rhinn M, Dierich A, Le Meur M, Ang S. 1999. Cell autonomous and non-cell autonomous functions of Otx2 in patterning the rostral brain. Development 126:4295–4304.

Soriano P. 1999. Generalized lacZ expression with the ROSA26 Cre reporter strain. Nat Genet 21:70–71.

Tajbakhsh S, Houzelstein D. 1995. In situ hybridization and beta-galactosidase: a powerful combination for analysing transgenic mice. Trends Genet 11:42.

Tallquist MD, Soriano P. 2000. Epiblast-restricted Cre expression in MORE mice: a tool to distinguish embryonic vs. extra-embryonic gene function. genesis 26:113–115.

Tucker AS, Al Khamis A, Sharpe PT. 1998. Interactions between Bmp-4 and Msx-1 act to restrict gene expression to odontogenic mesenchyme. Dev Dyn 212:533–539.

Varlet I, Collignon J, Robertson EJ. 1997. Nodal expression in the primitive endoderm is required for specification of the anterior axis during mouse gastrulation. Development 124:1033–1044.

Yamauchi Y, Abe K, Mantani A, Hitoshi Y, Suzuki M, Osuzu F, Kuratani S, Yamamura K. 1999. A novel transgenic technique that allows specific marking of the neural crest cell lineage in mice. Dev Biol 212:191–203.

Zambrowicz BP, Imamoto A, Fiering S, Herzenberg LA, Kerr WG, Soriano P. 1997. Disruption of overlapping transcripts in the ROSA beta geo 26 gene trap strain leads to widespread expression of beta-galactosidase in mouse embryos and hematopoietic cells. Proc Natl Acad Sci U S A 94:3789–3794.

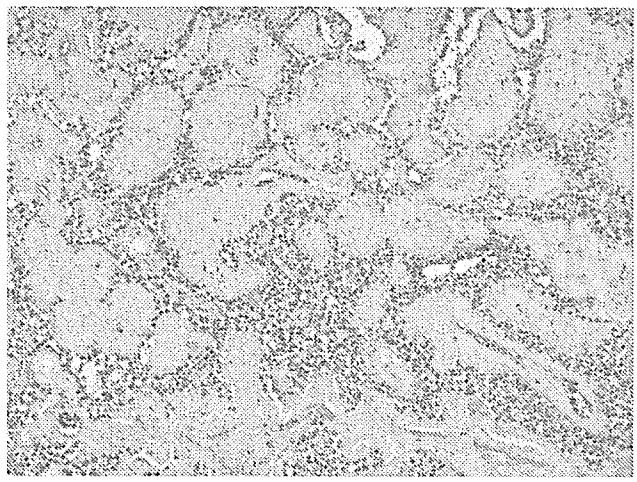

FIGURE 2. Solid pseudopapillary tumor of the pancreas: histological section from the resected tumor (Hematoxulin & Eosin stain, original magnification ×20). Specimen reveals bland cells, forming pseudopapillary structures, with focal hyalinization. There was no hemorrhage, necrosis, or significant mitotic activity.

EUS-guided FNA, which has only been reported in adults 3 other times in the literature.[4-6]

Cytological features of solid pseudopapillary tumors are distinct from those of other cystic or solid tumors of the pancreas. The cells are relatively bland with uniform, round to oval, eccentrically located nuclei with fine chromatin and a moderate amount of cytoplasm. Nuclear grooves are typical, and nucleoli are inconspicuous. Metachromatic hyaline globules may also be seen, as well as macrophages, multinucleated giant cells, cholesterol, and necrotic debris. The cytological findings for this tumor were unusual. The FNA of our case demonstrated moderate cellularity with cells that were round to oval with a more condensed distribution of chromatin. The cells were also small with scant cytoplasm and lacked nuclear grooves.

In conclusion, this case represents an unusual presentation of a rare pancreatic tumor. Both the clinical and pathologic presentations of this case were highly unusual. Surgical resection has generally been curative, but close follow-up is advisable, particularly with the histological characteristics that suggest a more aggressive tumor.[7]

Maria C. Uzquiano, MD*
Supriya Kuruvilla, MD*
Craig P. Fischer, MD†
Jing Liu, MD, PhD*
Savitri Krishnamurthy, MD‡
Douglas G. Adler, MD§
*Departments of Pathology and Laboratory Medicine
†Surgery, University of Texas Health Science Center Houston Medical School
‡Department of Pathology and Laboratory Medicine, M.D. Anderson Cancer Center
§Division of Gastroenterology and Hepatology, Department of Internal Medicine, University of Texas Health Science Center Houston Medical School
douglas.adler@uth.tmc.edu

REFERENCES

1. Gonzalez-Campora R, Rios Martin JJ, Villar Rodriguez JL, et al. Papillary cystic neoplasm of the pancreas with liver metastasis coexisting with thyroid papillary carcinoma. *Arch Pathol Lab Med.* March 1995;119(3): 268–273.
2. Wick MR, Graeme-Cook FM. Pancreatic neuroendocrine neoplasms: a current summary of diagnostic, prognostic, and differential diagnostic information. *Am J Clin Pathol.* June 2001;115(Suppl):S28–S45.
3. Tien YW, Ser KH, Hu RH, et al. Solid pseudopapillary neoplasms of the pancreas: is there a pathologic basis for the observed gender differences in incidence? *Surgery.* June 2005;137(6):591–596.
4. Bardales RH, Centeno B, Mallery JS, et al. Endoscopic ultrasound–guided fine-needle aspiration cytology diagnosis of solid-pseudopapillary tumor of the pancreas: a rare neoplasm of elusive origin but characteristic cytomorphologic features. *Am J Clin Pathol.* May 2004;121: 654–662.
5. Master SS, Savides TJ. Diagnosis of solid-pseudopapillary neoplasm of the pancreas by EUS-guided FNA. *Gastrointest Endosc.* June 2003;57(7):965–968.
6. Mergener K, Detweiler SE, Traverso LW. Solid pseudopapillary tumor of the pancreas: diagnosis by EUS-guided fine-needle aspiration. *Endoscopy.* December 2003; 35(12):1083–1084.
7. Huang HL, Shih SC, Chang WH, et al. Solid-pseudopapillary tumor of the pancreas: clinical experience and literature review. *World J Gastroenterol.* March 7, 2005; 11(9):1403–1409.

Enhanced Trypsin Activity in Pancreatic Acinar Cells Deficient for Serine Protease Inhibitor Kazal Type 3

To the Editor:

Acute pancreatitis is a severe inflammatory disorder of the pancreas, which is believed to be caused by autodigestion of the pancreas by its own digestive enzymes. However, digestive enzymes are secreted from the pancreas as inactive precursor zymogens and are normally activated only in the duodenum. Thus, premature protease activation should occur in the pancreas to trigger pancreatitis. Because conversion of trypsinogen to trypsin is the trigger for protease activation, control of trypsin activity is important to prevent the development of acute pancreatitis.

In human, trypsin activity is thought to be predominantly controlled by the serine protease inhibitor, Kazal type 1 (SPINK1), which is also known as a pancreatic secretory trypsin inhibitor. In mouse, this homologous gene is designated as *Spink3* (serine protease inhibitor, Kazal type 3). The SPINK1 is synthesized in acinar cells of the pancreas and is thought to inhibit up to 20%

© 2006 Lippincott Williams & Wilkins

Copyright © Lippincott Williams & Wilkins. Unauthorized reproduction of this article is prohibited.

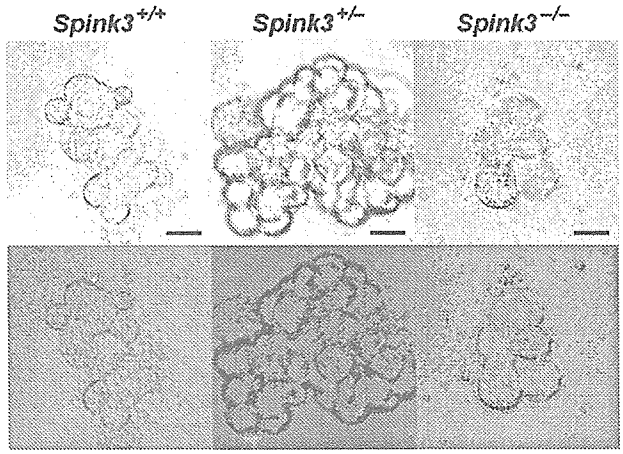

FIGURE 1. Detection of intraacinar trypsin activity using (CBZ-Ile Pro-Arg)$_2$-rhodamine 110 as a substrate. Isolated acini of each genotypes at 0.5 days after birth were prepared by collagenase digestion, and then placed under a coverslip for intracellular fluorescence imaging after exposure to the cell permeant fluorogenic substrate (CBZ-Ile-Pro-Arg)$_2$-rhodamine

of the trypsin in the pancreas by binding to the catalytic site of trypsin.[1] Thus, a lack of SPINK1 activity may result in the failure of suppression of prematurely activated trypsin within the acinar cells, leading to autodigestion of the exocrine pancreas by activated proteases.

To examine this possibility, we had previously generated serine protease Kazal type 3 (Spink3)-deficient mice.[2] In this study, trypsin activity in the pancreas of *Spink3*$^{-/-}$ mice was not increased, but was almost equal to that in wild-type and heterozygous mice, when free trypsin activity was measured by using benzoyl-l-arginine *p*-nitroanilide as chromogenic substrate, However, we postulated that this method was not sensitive enough to detect a low level of trypsin activation. Thus, we decided to examine trypsin activity using a synthetic trypsin substrate, (CBZ-Ile-Pro-Arg)$_2$-rhodamine 110, a more sensitive method than that using benzoyl-l-arginine *p*-nitroanilide. This method that permits observation of premature, intracellular activation of serine-proteases directly in living, functionally intact pancreatic acinar cells was developed by Krüger et al.[3]

The Spink3-deficient mice at 0.5 and 1.5 days after birth were killed and the pancreas was immediately removed. Acini from animals were freshly prepared by collagenase digestion,[4] then suspended in Hepes (24.5 mM) buffered medium (pH 7.5) containing NaCl (96 mM), KCl (6 mM), $MgCl_2$ (1 mM), NaH_2PO_4 (2.5 mM), $CaCl_2$ (0.5 mM), glucose (11.5 mM), Na-pyruvate (5 mM), Na-glutamate (5 mM), Na-fumarate (5 mM), minimum essential medium (1% vol/vol), and bovine serum albumin, fraction V (1% wt/vol). To study intracellular trypsin activity in living acini, they were left to equilibrate for 30 minutes at 37°C. Cells were suspended in the medium in the presence of the synthetic trypsin substrate (CBZ-Ile-Pro-Arg)$_2$-rhodamine 110 (10 μM; Molecular Probes, Eugene, Ore). Bisamide derivatives of rhodamine 110 are extremely sensitive molecular probes, 50- to 300-fold more so than the analogous coumarin-based substrate,[5] and selective substrates can be used for assaying proteinases in solution or inside living cells. Trypsin activity could be directly observed when living acini were placed under a fluorescence microscope (Olympus AX70, CCD-camera DP70 with a U-MWIG2 filter; Olympus, Hamamatsu, Japan) at an excitation wave length of 520 to 550 nm and an emission wave length of 580 nm.

We could detect trypsin activity in Spink3-deficient pancreatic acinar cells at 0.5 (Fig. 1) and 1.5 (data not shown) days after birth. On the other hand, trypsin activity was not detected in pancreatic acinar cells of *Spink3*$^{+/+}$ and *Spink3*$^{+/-}$ mice. These findings suggest that a small amount of trypsinogen is activated into trypsin within acinar cells, and that Spink3 is the main molecule controlling trypsin activity in acinar cells. The inability, in our previous study,[2] to detect trypsin activity in the pancreas of *Spink3*$^{-/-}$ mice using benzoyl-l-arginine *p*-nitroanilide as a substrate, may have been due to the low sensitivity of assay system.

In physiological conditions, digestive enzymes are stored as inactive precursor zymogens in pancreatic acinar cells. Hence, considerable interest has been focused on the mechanisms by which those enzymes become prematurely activated within the pancreas, and so leading to pancreatic injury. Trypsinogen may also be activated by the lysosomal cysteine protease cathepsin B[6,7] or by autoactivation in acidic environments.[6,8] However, the mechanism responsible for the intraacinar activation of trypsinogen is thought to be complex and has not been fully elucidated. Although we could not define this mechanism, we clearly demonstrated that a small amount of trypsinogen can be activated to trypsin in acinar cells in the absence of Spink3.

In *Spink3*$^{-/-}$ mice, excessive autophagy appeared and the rapid onset of cell death occurred in the pancreas within a few days after birth.[2] Presently, it is not clear whether a low level of trypsin activation is the trigger for abnormal autophagy. Even though a low level of trypsin activation can cause autophagy, it is difficult to imagine that autophagy can proceed to occupy the whole cytoplasm to cause cell death. In any case, the present results clearly demonstrated that the loss of Spink3 resulted in the failure of control of trypsin activation in acinar cells. It is possible that mutation of the *SPINK1* gene may result in the failure to inhibit activated trypsin in the human pancreas, leading directly to pancreatitis or a potentiation of the harmful effect to the pancreas by other genetic or environmental insults.

© 2006 Lippincott Williams & Wilkins

Copyright © Lippincott Williams & Wilkins. Unauthorized reproduction of this article is prohibited.

Masaki Ohmuraya, MD, PhD*†
Masahiko Hirota, MD, PhD†
Kimi Araki, PhD*
Hideo Baba, MD, PhD†
Ken-ichi Yamamura, MD, PhD*
*Division of Developmental Genetics
Institute of Molecular Embryology
and Genetics
†Department of
Gastroenterological Surgery
Kumamoto University
Kumamoto, Japan
yamamura@gpo.kumamoto-uc.ac.jp

REFERENCES

1. Rinderknecht H. Pancreatic secretory enzymes. In: Go VLW, Di-Magno JD, Gardner JD, Lebenthal E, Reber HA, Scheele G eds. *The pancreas: biology, pathophysiology, and disease.* New York, NY: Raven Press, 1993:219–251.
2. Ohmuraya M, Hirota M, Araki M, et al. Autophagic cell death of pancreatic acinar cells in serine protease inhibitor Kazal type 3-deficient mice. *Gastroenterology.* 2005;129:696–705.
3. Krüger B, Lerch MM, Tessenow W. Direct detection of premature protease activation in living pancreatic acinar cells. *Lab Invest.* 1998;78:763–764.
4. Grosfils K, Métioui M, Tiouli M, et al. Isolation of rat pancreatic acini with crude collagenase and permeabilization of these acini with streptolysin O. *Res Commun Chem Pathol Pharmacol.* 1993;79:99–115.
5. Leytus SP, Melhado LL, Mangel WF. Rhodamine-based compounds as fluorogenic substrates for serine proteinases. *Biochem J.* 1983;209:299–307.
6. Figarella C, Miszczuk-Jamska B, Barrett AJ. Possible lysosomal activation of pancreatic zymogens. Activation of both human trypsinogens by cathepsin B and spontaneous acid. Activation of human trypsinogen 1. *Biol Chem Hoppe Seyler.* 1988;369:293–298.
7. Greenbaum LM, Hirshkowitz A, Shoichet I. The activation of trypsinogen by cathepsin B. *J Biol Chem.* 1959;234:2885–2890.
8. Kassell B, Kay J. Zymogens of proteolytic enzymes. *Science.* 1973;180:1022–1027.

Discussion on Applicability of Disseminated Intravascular Coagulation Parameters in the Assessment of the Severity of Acute Pancreatitis

To the Editor:

The study published by Dr Maeda et al[1] contributes to our better understanding of the role osf the disorders of hemostatic system during the severe acute pancreatitis (SAP). Although first studies dealing with this problem were done in the early sixties of the last century,[2] this topic has not attracted much attention. However, during the last 15 years, the role of disorders of hemostasis during the course of SAP was highlighted, especially in the development of accompanied early and late systemic complications, using new findings related to pathophysiology of hemostatic system and new specific methods for analyzing single factors of the hemostatic system.

Systemic inflammation with consecutive high levels of proinflammatory cytokines in the circulation, among other things, affects hemostatic system during SAP. Expression of tissue factor that is followed by the activation of extrinsic pathway initiated coagulation. This leads to hypercoagulative state with impaired fibrinolysis. Overwhelming activation of this process often results in microthrombus formation, and in interaction with a severe inflammatory reaction, it may result in microvessel obstruction, microbleeding, and malcirculation of the tissue. There is lot of evidence that inflammation and coagulation are closely related processes, which considerably affect each other.

Dr Maeda et al[1] by measuring disseminated intravascular coagulation parameters (according to the Japanese classification) showed clearly that levels of particular disseminated intravascular coagulation parameters on admission to the hospital correlate with fatal outcome in patients suffering from SAP. According to receiver operating characteristic analysis, levels of antithrombin III have been the most accurate predictor of death. These findings corroborate our previously published results which suggested that decreased plasma levels of activity of protein C and antithrombin III, and increased plasma concentrations of D-dimer and plasminogen activator inhibitor type I are associated with poor outcome of surgically treated patients with SAP.[3]

However, it seems that for optimal management of these patients, early prediction of severity could be as important as the prediction of outcome. In the last several years, some studies have pointed out the role of measurement of early hemostatic disturbances in the prediction of severity of SAP. Salmone et al[4] reported that levels of D-dimer on admission 4 times higher than upper limit may be considered a reliable sign of SAP. Ottesen et al[5] have demonstrated in an experimental study that during the first hours of illness only levels of protein C, among other measured parameters of hemostasis, differ significantly between animals with necrotizing pancreatitis and control group. Very recently, Finish group[6] showed the association of protein C pathway with inflammatory regulation in SAP. During the first 2 weeks of hospitalization, low levels of protein C was observed in 92% of patients with multiple organ dysfunction syndrome and in 44% of control patients with SAP but without multiple organ dysfunction syndrome.

In the study of Dr Maeda et al,[1] measurement of activity of protein C was not done. That might be the only lack of this very well designed study. Protein C is, up to now, the only known parameter of hemostasis for which it is proven that it acts as anti-inflammatory, anticoagulant, and profibrinolytic factor. Among the studies that have shown the importance of measurement of protein C for the early prediction of severity of acute pancreatitis (AP), there is some evidence of therapeutic effects of application of recombinant activated protein C (rAPC) in treatment of these patients. In addition, PROWESS study[7] demonstrated a significant improvement of survival on administration of rAPC to sepsis patients. Sixty-two patients (7.3%) with septic complications of SAP have been included in this study. Among them, 29 patients have been treated with rAPC, whereas 33 patients were in placebo group. The analysis of results has shown the decrease of the relative risk of death for approximately 43%. Machala et al[8] have reported positive experience with application of rAPC on the 2 patients with septic complications during SAP. Discontinuation of the therapy and fast elimination of the drug, which could be enormously important during the treatment of patients with SAP, have enabled planned invasive procedures (surgical intervention and smaller therapeutic procedures) to be done without increased

© 2006 Lippincott Williams & Wilkins

Copyright © Lippincott Williams & Wilkins. Unauthorized reproduction of this article is prohibited.